Time-resolved excitation and ionization of a laser-pumped Ba vapor

L. Jahreiss and M. C. E. Huber
Physical Chemistry Laboratory and Institute of Astronomy, Swiss Federal Institute of Technology Zurich (Eidgenössische Technische Hochschule Zürich), ETH-Zentrum, CH-8092 Zürich, Switzerland
(Received 11 July 1983)

The excitation and ionization of barium vapor by resonant laser irradiation was investigated in detail. Measurements were taken on a moderately dense vapor (10^{19} to 10^{21} m^{-3}) that was illuminated by an intense (7 GW m^{-2}) 1-μs-long dye-laser pulse. The laser was tuned to the Ba resonance line at $\lambda = 553.5$ nm, and burned through the 0.25-m-long vapor column in less than 50 ns. The excitation histories of twelve Ba and Ba^+ levels were determined with a time resolution of 5 ns by use of hook-interferometry spectra. The emission, which reflected the population of high-lying levels, was also analyzed. For the higher densities investigated, almost complete ionization was achieved within 400 ns. Ionization was highly density-dependent and this pointed to collision-dominated ionization mechanisms. Strontium atoms—present as an impurity in the Ba vapor, yet not in resonance with the laser radiation—were also found to ionize rapidly. This provided further confirmation of the dominance of collisions. We established that seed electrons were heated in superelastic collisions with laser-excited atoms, and that subsequent electron-impact excitation and ionization, as well as photoionization of high-lying levels lead to the creation of more electrons. Electron density and concomitant ionization then increase rapidly. The observed transfer of the excitation energy to the electrons by superelastic collisions requires contributions not only from the laser-pumped resonance level, but also from the lower-lying metastable Ba levels. These are, in fact, populated very rapidly and efficiently via the resonance level.

I. INTRODUCTION

Lucatorto and McIlrath discovered in 1976 that excitation of dense vapors with resonant laser radiation leads to rapid ionization.[1] To date this effect has been explored by use of the elements Li,[2] Na,[1,3–9] Ca,[10] Sr,[10–12] and Ba,[10,13–18] at densities ranging from 10^{18} to 10^{22} m^{-3}. Several authors concur with the conjecture[2] that the dominant energy transfer from laser-excited atoms takes place by superelastic collisions, i.e., by a process originally proposed by Measures in 1970.[19] Such collisions provide rapid heating for a few free electrons, which are initially created by comparatively inefficient seed processes.[19–21] The resulting "hot" electrons then are capable of producing more free electrons, and this results in the observed ionization. Other authors claim that two-photon processes play an important role in the ionization[13–15] or that the trapped resonance radiation gives rise to multiphoton processes.[4] The latter view, however, is controversial.[22,23]

Supporting evidence for the opinion that superelastic collisions with laser-excited atoms are a dominant mechanism in the ionization of dense vapors was reported by Skinner.[10] He had excited mixtures of barium and strontium vapors and had found (1) a strong density dependence of the ionization efficiency and (2) a more efficient ionization of barium when he pumped the Sr rather than the Ba resonance line. Both these findings point to collisions being responsible for the energy transfer of the laser excitation.

No ionization could be detected by Bowen and Thorne[16,17] in their laser-excited Ba vapor. It is thought that the narrow-band pump-laser pulse resulted in coherent excitation and that the lack of ionization is probably also a consequence of the short pulse length.

Lucatorto and McIlrath[18] have also demonstrated that Ba^+—ionized by resonant laser excitation—could be ionized again to Ba^{2+}, by irradiation with a second laser pulse tuned to a resonance line of Ba^+. Here the ionization potential was nearly 4 times larger than the energy of the resonant photon, while in the prior investigations on neutral vapors it had only been about 2 to 3 times as large. As a consequence, one—maybe even two—additional collisions or coincident photons are required for many of the possible ionization paths: associative and Penning ionization, multiphoton ionization, or stimulated Raman scattering with subsequent photoionization. Since the corresponding ionization rates then become negligible, such processes cannot be relevant contributors to ionization, and heating of the free electrons by superelastic collisions remains as the likely process leading to the rapid and complete ionization. Given the fact that copious free electrons with Maxwell distribution are initially present in Ba^+, the interpretation according to the superelastic-collision model of Measures *et al.*[19–21] is straightforward, in contrast to the case of neutral vapors.

In related experiments, electrons were identified which had undergone superelastic collisions with a laser-excited beam containing Na atoms in the $3p$ level[24] and Ba atoms in the $5d\ ^1D_2$ and $6p\ ^1P_1^o$ levels.[25] In the case of Na, up to three consecutive superelastic collisions were observed.

Extensive investigations of laser-excited sodium in the density range 10^{18}–10^{22} m^{-3} have also been reported by Carré, Roussel, and colleagues.[5–8] At low densities (10^{18}–10^{19} m^{-3}) they found the ionization rate to be dominated by laser-modified and laser-assisted associative ionization as well as by laser-assisted Penning ionization. Other seed processes, as, for example, two-photon ionization and energy-pooling collisions, were judged to be negligible. At higher densities (10^{19}–10^{21} m^{-3}) the energy gain of electrons by superelastic collisions took over and the model of Measures *et al.*[19–21] again provided an explanation for the total ionization observed to occur at a density of 2×10^{20} m^{-3}.

Additional experiments on the ionization efficiency of sodium vapors in the presence of various buffer gases at different pressures (He,Ne,Ar; 0.1 to 500 Torr, i.e., ≈ 10 to 7×10^{4} Pa) have been performed by Stacewicz and Krasinski.[9] Under the conditions of the short (10-ns) laser pulses used, a strong dependency on the buffer gas and its pressure was observed and explained by a reduced lifetime of the resonance level owing to pressure broadening. Energy loss of electrons in elastic collisions (with buffer-gas atoms or NaAr quasimolecules), and diffusion of the atoms out of the laser-excited zone—a process whose speed depends on the buffer-gas pressure—were found less important.

It was the aim of the present experiment to observe and quantitatively discuss the dominant processes leading to ionization by resonant laser excitation in barium. To this end, we irradiated Ba vapors with a 1-μs-long laser pulse, whose wavelength was tuned to the wavelength of the Ba resonance line ($\lambda=553.5$ nm), and followed the population dynamics with a time resolution of 5 ns. In particular, we determined the population history of 12 low-lying levels of neutral and ionized barium by use of time-resolved hook spectra.[26,27] We also analyzed the emission from high-lying levels of the barium atom.

We could prepare uniformly excited 0.23-m-long vapor columns in the density range 10^{19}–10^{21} m^{-3}, since we succeeded in burning through the column within less than 50 ns. This facilitated the diagnostics as compared with earlier experiments where an inhomogeneous layer was present[2,18] and models had to be used to determine densities in the excited part of the vapor column.[13–15] Our results can be interpreted in terms of heating of free electrons by superelastic collisions with the laser-excited atoms, with subsequent electron-impact excitation and ionization as well as photoionization of high-lying levels.

II. EXPERIMENT

Figure 1 shows the arrangement of our experiment as a block scheme: a flash-lamp pumped dye laser, tuned to the Ba resonance line ($\lambda=553.5$ nm), excited a barium vapor in the furnace. Vapor and furnace were also part of a hook-method[26] setup, which provided the main diagnostics.[27] This apparatus which comprised a continuum background source (viz., a second, N_2-laser pumped dye laser with broadband output), a Mach-Zehnder interferometer with compensation plate, and a stigmatic 3.4-m spectrograph enabled us to observe the anomalous dispersion in the vicinity of spectral lines, and thus to determine the densities of various atomic and ionic levels in the laser-excited vapor.

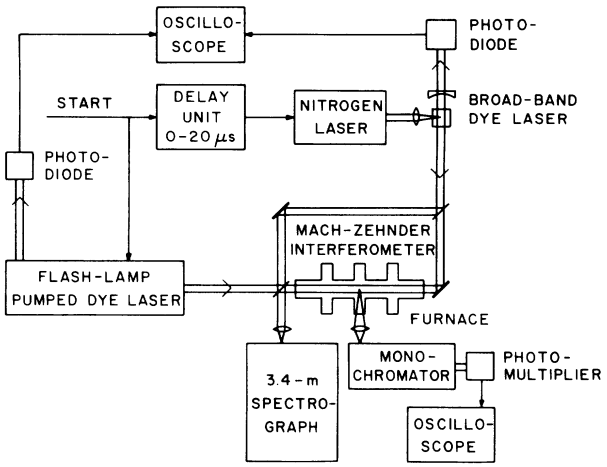

FIG. 1. Experimental arrangement.

The laser pulse that excited the Ba vapor was 1 μs long. The light pulse used for diagnostics by the hook method, on the other hand, had a duration of only 1 ns. By triggering this second laser with various delays we could thus sample the dynamics of the populations in the furnace with high time resolution. Photographs of the hook spectrum were taken in single-shot exposures on the 3.4-m spectrograph, and the actual delay of the pulse from the broadband laser was determined by use of a 100-MHz oscillograph (Tektronix 7633) that recorded the two laser outputs as signals from two photodiodes (Hewlett-Packard HP-5082-4205). The timing of a given density measurement with respect to the laser pulse exciting the vapor could thus be determined with a precision of 5 ns.

Since the hook method diagnostic, which is most suitable for strong lines, gave access only to the populations of relatively low-lying levels, we monitored the densities of higher-lying levels by observing the emission of the laser-excited vapor through a sidearm in the furnace. We measured the emitted radiation by means of a radiometrically calibrated spectrometer with a photomultiplier and recorded the resulting signal on an oscillogram as a function of time for a number of wavelengths.

The dye laser used for exciting the Ba vapor (DL-15B, Phase-R Co.) had a triaxial arrangement consisting of a coaxial flash lamp with an inner diameter of 15 mm and two coaxial dye cells that were separated by a centered fused silica tube of 4-mm inner diameter. The oscillating dye (a 8×10^{-5} molar aqueous solution of Fluorol-7GA with admixtures of Ammonyx LO and Cyclooctatetraen[28]) was circulating in the innermost cell and was surrounded by another dye circulating between the flash lamp wall and the inner tube. The outer dye (a 2×10^{-4} molar solution of Coumarin 440 dye in methanol) had an emission maximum coinciding with the absorption maximum of the inner dye. The triaxial arrangement prevented the laser dye from rapidly degrading under the ultraviolet ir-

radiation of the flash lamp and—more importantly—permitted a better control of the dye temperatures. This improved the laser beam quality and enhanced the output energy by about 50%.[29]

The laser cavity was 1.25 m long and comprised a plane output mirror with 20% reflectance, a beam expander (5 times), a Fabry-Perot interferometer with a free spectral range of 0.5 nm and coatings with 30% reflectance, and a 1200-line/mm plane grating. The electrical input to the flash lamp (250 J) resulted in a 100-mJ laser pulse with a rise time of 170 ns, a full width at half maximum (FWHM) of 750 ns, and a peak power of 0.14 MW. The laser output had a spectral bandwidth of 15 pm and a beam diameter and divergence of 4 mm and 1 mrad, respectively. By use of a lens ($f=1.7$ m) we focused the beam to a diameter of 3.2 mm in the center of the furnace, so that the peak irradiance reached 7 GW m^{-2}. When needed, the laser output could be attenuated by neutral density filters.

The radiation had a linear polarization of $\approx 90\%$. Since the dielectric beam splitters of the Mach-Zehnder interferometer had a transmission of 85% for the predominant direction of the polarization, nearly the entire laser energy was transmitted into the furnace.

The energy of the laser pulses was measured with a thermopile radiometer (type-14NO, Laser Instrumentation Ltd., Chertsey, Surrey, England), which has an accuracy stated to be 3%. An additional measurement for comparison carried out with a pyroelectric joulemeter (model J3 of Molectron Corp.) was within the estimated absolute accuracy of 20%. For convenience, the transmission of the optical system (consisting of two mirrors, one lens, and one beam splitter) that directed and focused the pump laser into the furnace, was measured once; subsequently the laser pump energy was always determined by a measurement of the actual laser output.

Spectral interferograms displaying the anomalous dispersion—the hook spectra—were recorded in the focal plane of the Ebert mounted, stigmatic 3.4-m spectrograph (Jarrell-Ash Co.). A 600-line/mm grating diffracting into third order resulted in a plate factor of about 0.147 nm/mm and in a resolution limit of ≈ 10 pm on the Polaroid film (type 667, 3000 ASA) used to photograph the hook spectra.

The ratio between length and width of the Mach-Zehnder interferometer was chosen to be 2,[30] and the fringes were localized in the center of the furnace. The fringes could then be adjusted by turning a single interferometer element, viz., the mirror in the reference arm, and were always imaged on the entrance slit of the stigmatic 3.4-m spectrograph. In this way we also obtained information on the density distribution across the excited vapor column.[31]

The entire hook-method apparatus was illuminated by continuum radiation from an untuned dye laser that was pumped by a home-built nitrogen laser. The continuum had a bandwidth of 15—35 nm and a central wavelength in the range of 417—608 nm, depending on the particular dye used. The cavity—consisting of a tilted dye cuvette of rectangular cross section and an Al-coated concave mirror (with a 25-mm radius of curvature)—was left incomplete (i.e., without an output mirror), in order to suppress spectral structure in the continuum.

The furnace, finally, was a conventional, electrically heated spectroscopic furnace made out of a stainless-steel tube with 50-mm inner diameter. Windows placed on sidearms at three locations along the hot zone permitted observations of the resonance fluorescence and the radiation emitted by the decay of other excited levels of the laser-pumped vapor column. Several layers of a fine stainless-steel mesh lining the furnace wall hindered the molten Ba metal from rapidly flowing to the water-cooled furnace ends. To reduce the vapor flow to the cooler parts of the furnace we used Ar buffer gas at 40 Torr (i.e., 5.3×10^3 Pa), and had diaphragms with central 4-mm apertures inserted at the ends of the 0.23-m-long hot zone. By use of a set of baffles, in particular conical, water-cooled baffles at the ends of the furnace and in the sidearms,[32] the coating of the windows by Ba could be suppressed at our normal operating conditions (870 °C).

The temperature was measured with four NiCr-Ni thermocouples which were placed on the outside wall of the furnace tube. We determined the actual column density by spectroscopic means. At a temperature of 870 °C, and with an Ar buffer-gas pressure of 5.3×10^3 Pa, we found a column density of 1.5×10^{20} m^{-2}. If we assume an effective column length of 0.23 m, this corresponds to a density of 6.5×10^{20} m^{-3} (or about 17 times less than the density read off a vapor-pressure curve). At a fixed furnace heating-power, the density of the barium vapor was stable: the observed drifts in column density remained below 10% per hour.

III. EXPERIMENTAL RESULTS

In our experiment we have measured the time-dependent densities of most of the barium levels and configurations shown in Fig. 2. The population dynamics of the low-lying levels in both, neutral and ionized barium were determined from time-resolved anomalous-dispersion measurements. The densities of configurations lying above 2.5 eV were derived from calibrated spectral emission measurements. In supplementary observations we also detected stimulated infrared radiation in transitions that connect the laser-pumped $6s6p\ ^1P_1^o$ level with metastable levels.

Furthermore, we monitored the excitation of the strontium and calcium atoms that were present as impurities in the barium vapor. Since those atoms are not in resonance with the pump laser, they provide an opportunity to separately observe effects of collisional excitation.

Measurements were taken with laser irradiances and Ba ground-state densities ranging over a factor of 10 (0.7—7 GW m^{-2}) and a factor of 100 (10^{19}—10^{21} m^{-3}), respectively.

In the following sections we will first describe the results obtained from anomalous-dispersion measurements with the different laser powers used. Subsequently, we will discuss the effect of varying the vapor density and the concomitant changes in ionization efficiency. After the

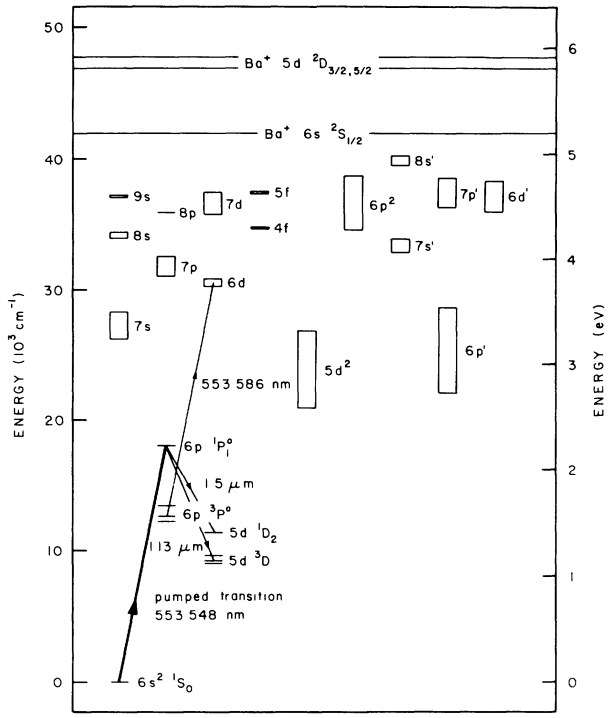

FIG. 2. Summary level diagram.

ensuing description of our emission measurements and some comments on additional measurements and observations, we shall conclude the section with a critical comparison between our experimental conditions and those used in previous experiments.

A. Time-resolved hook-interferometry measurements

The evaluation of the hook interferograms uses the following formula[26,27]:

$$\int_0^{l'} N_i(z)dz = \frac{\pi K}{r_0 \lambda_{ij}^3 f_{ij}} \Delta_{ij}^2 = \bar{N}_i l \ , \tag{3.1}$$

where $N_i(z)$ is the population density of the level i depending on the position z on the optical axis and l' the length of the oven. $K = p\lambda'/\Delta\lambda$ is the hook-interferogram constant (that can be determined from the number p of interference fringes in a line-free wavelength interval $\Delta\lambda$ at a wavelength λ'), $r_0 = e^2/4\pi\epsilon_0 m_e c^2 = 2.82\times10^{-15}$ m is the classical electron radius, and λ_{ij}, f_{ij}, and Δ_{ij} are the wavelength, absorption oscillator-strength, and hook separation of the transition $i \rightarrow j$, respectively.

As the absorbing vapor column is not homogenous, only the column density $\bar{N}_i l$ can be determined with (3.1). However, from the length of the heated zone of the furnace, an effective length l of the vapor column and a corresponding average density $\bar{N}_i$ can be estimated.

Interferograms of good quality were obtained as long as the beams of both, the pump and the background dye lasers were uniform and reproducible.[10] With these precautions strong inhomogeneities in the interferograms could be avoided.[31,33] And it was often possible to exploit the hook-vernier technique[34] for determining small hook separations.

Our time-resolved hook-interferometry measurements comprised the following barium levels (cf. Fig. 2): In Ba, $6s^2\,{}^1S_0$, $5d\,{}^3D_{1,2,3}$, $5d\,{}^1D_2$, $6p\,{}^3P^o_{0,1,2}$, $6p\,{}^1P^o_1$; in Ba^+, $6s\,{}^2S_{1/2}$, $5d\,{}^2D_{5/2}$, $6p\,{}^2P^o_{3/2}$. Strontium as well as calcium, which are present only as small impurities in solid barium, appear in the furnace with vapor densities corresponding to, respectively, $\approx 10\%$ and 0.2% of that of barium. As a consequence, we could also obtain time-resolved hook measurements for atomic systems that were not coupled to the strong radiation field in the Ba resonance line. The following levels could be observed: in Sr, $5s^2\,{}^1S_0$, $5p\,{}^3P^o_2$; in Sr^+, $5s\,{}^2S_{1/2}$; in Ca, $4s^2\,{}^1S_0$. The atomic data used to derive the column densities of the above levels are listed in Table I.

In Figs. 3–9 the results are given for a fixed density and for three different laser powers. The column density $\bar{N}l$ of the Ba ground state was 1.46×10^{20} m^{-2} ($\pm 6\%$); with an estimated $l = 0.23$ m an average Ba density $\bar{N} = 6.3\times10^{20}$ m^{-3} may be assumed. The three power levels used were 100%, 30.5%, and 10.1% of the full power (7 GW m^{-2}). Results for higher densities $\bar{N}l = 2.23\times10^{20}$ m^{-2} ($\pm 6\%$) are given in Fig. 10, and the dependence of the ionization efficiency at full laser irradiance is shown in Fig. 11.

In the course of the data reduction with the published f values given in Table I, we noted that the sum of the population densities of all levels at short delay times ($t \approx 50$ ns) was only about 50% of the initial ground-state density. For larger delays (> 300 ns), when the barium was almost completely ionized, the sum approached 100% again. An obvious conclusion was therefore that the oscillator strengths of absorption lines originating from the low-lying excited Ba levels (which were predominantly populated at $t \approx 50$ ns) were too large by a factor of 2, whereas those of the Ba ion were correct. Since a comparison of the oscillator strengths in question with recent lifetime measurements in Ba led to very similar conclusions, we corrected some of the f values as shown in Table I. A detailed discussion of these corrections[35] is given in a separate paper.[36]

As the Ba I line, $6p\,{}^3P^o_1 - 6d\,{}^3D_1$, at $\lambda = 553.586$ nm is only 38 pm away from the resonance line (see Fig. 2) it was also excited by the pump laser. This resulted in an efficient population of the level $6d\,{}^3D_1$ (cf. Fig. 12) which subsequently could lead to direct ionization. To minimize the influence of this ionization channel, the pump laser was always tuned to about 553.52 nm. As the equivalent width of the resonance line is about 0.5 nm at our column densities, this detuning has no influence on the pumping efficiency of the resonance level.

The laser pulse shown in Fig. 3 was reproducible to about 2% for successive pulses. During an experiment lasting several hours, however, the energy of the laser pulses could fall by about 20% because the dye was degrading. Data were therefore normalized to an average pulse form by correcting the measured delay times so that equal delay times correspond to equal accumulated energy inputs. Since the ground-state density was observed to fluctuate by $\approx 10\%$ about the time-averaged density, the level populations are also normalized to an average

TABLE I. List of lines used with the hook method.

	Transition	λ (nm)	f_{lit}	f_{corr}[a]
Ba I	$6s^2\,^1S_0-6s6p\,^1P_1^o$	553.548	1.59[b]	1.64
	$6s^2\,^1S_0-5d6p'\,^3D_1^o$	413.243	0.0099[b]	0.0102
	$6s6p\,^1P_1^o-6s8d\,^1D_2$	487.765	0.60[c]	0.31
	$6s6p\,^1P_1^o-5d6d'\,^3P_2$	494.735	0.167[c]	0.085
	$6s5d\,^3D_1-5d6p'\,^3P_0^o$	601.947	0.26[b]	0.15
	$6s5d\,^3D_2-5d6p'\,^3P_1^o$	606.312	0.32[b]	0.18
	$6s5d\,^3D_3-5d6p'\,^3P_2^o$	611.078	0.40[b]	0.22
	$6s5d\,^1D_2-5d6p'\,^1P_1^o$	582.628	0.30[b]	0.13
	$6s6p\,^3P_0^o-6p^2\,^3P_1$	443.189	1.1[b]	0.50
	$6s6p\,^3P_1^o-6p^2\,^1D_2$	440.254	0.34[b]	0.15
	$6s6p\,^3P_2^o-6p^2\,^3P_2$	452.317	0.29[b]	0.13
	$6s6p\,^3P_2^o-6s6d\,^3D_3$	577.762	1.0[b]	0.45
	$6s6p\,^3P_2^o-6s6d\,^3D_2$	580.023	0.24[b]	0.08
Ba II	$6s\,^2S_{1/2}-6p\,^2P_{3/2}^o$	455.403	0.74[b]	
	$6s\,^2S_{1/2}-6p\,^2P_{1/2}^o$	493.409	0.35[b]	
	$5d\,^2D_{5/2}-6p\,^2P_{3/2}^o$	614.172	0.14[b]	
	$6p\,^2P_{3/2}^o-6d\,^2D_{5/2}$	413.065	1.2[b]	
Sr I	$5s^2\,^1S_0-5s5p\,^1P_1^o$	460.733	1.92[d]	
	$5s5p\,^3P_2^o-5s5d\,^3D_3$	496.226	0.41[e]	
Sr II	$5s\,^2S_{1/2}-5p\,^2P_{1/2}^o$	421.552	0.34[f]	
Ca I	$4s^2\,^1S_0-4s4p\,^1P_1^o$	422.673	1.75[d]	

[a]The oscillator strengths used in this work were corrected (Refs. 35 and 36).
[b]Reference 37.
[c]Reference 14.
[d]Reference 38.
[e]Value from Ref. 39 adapted to a more recent measurement of the f value of the resonance line (Ref. 38).
[f]Reference 40.

ground-state density.

The errors of the column densities given in our figures reflect not only the measurement uncertainties but also the reproducibility of different experiments made under nominally identical conditions. Uncertainties in the f values, on the other hand, are not included in the error bars, since the f-value scale has no influence on the time behavior of a population. The errors on the time scale represent the uncertainty in measuring the interval between the two photodiode pulses on the oscilloscope. All measurements shown in Figs. 3—12 were carried out with 40 Torr (5.3×10^3 Pa) of argon as a buffer gas.[41]

The measured time-resolved population densities were drawn as continuous curves in the figures although they consist of about 30 measured points. As an example, we indicated the actual data points for the level $5d\,^1D_2$ in Fig. 3.

1. *Measurements taken at full laser irradiance (7 GW m^{-2}, Figs. 3—7)*

Figure 3 shows the time-dependent populations of the levels $6s^2\,^1S_0$, $6p\,^1P_1^o$, and $5d\,^1D_2$ as well as the shape of the pump-laser pulse. To measure the ground-state densi-

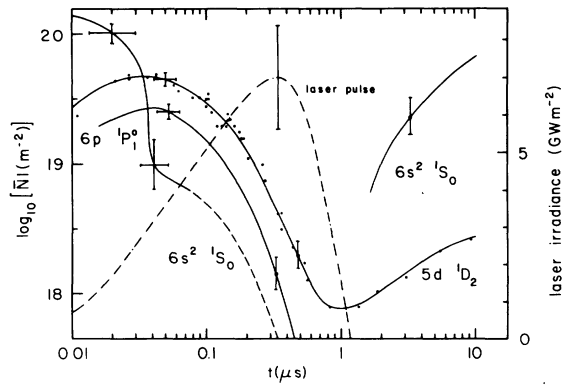

FIG. 3. Logarithmic population histories of the Ba ground state ($6s^2\,^1S_0$), the laser-pumped level ($6p\,^1P_1^o$) and a metastable level ($5d\,^1D_2$). The absolute column densities $\bar{N}l$ were determined by time-resolved hook measurements. Each curve is defined by ≈30 data points, as exemplified for the case of the $5d\,^1D_2$ level. The ground-state column density before the laser pulse was $\bar{N}_0 l = 1.46\times10^{20}$ m^{-2} (corresponding to $\bar{N}_0 \simeq 6.3\times10^{20}$ m^{-3}). Argon at 5.3×10^3 Pa (40 Torr) was present as a buffer gas. The pump laser whose pulse shape is also shown, produced a peak irradiance in the furnace of 7 GW m^{-2} (right-hand ordinate).

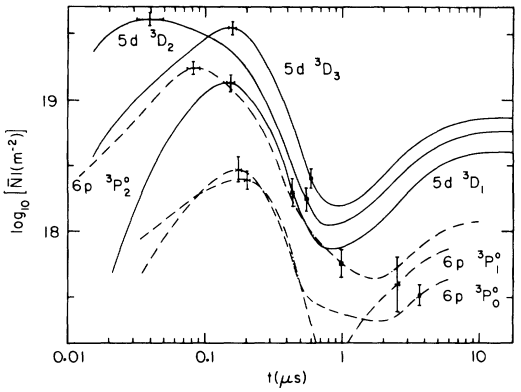

FIG. 4. Logarithmic population histories for the metastable Ba levels $5d\,^3D_{1,2,3}$ (——) and $6p\,^3P^o_{0,1,2}$ (—·—·). Experimental conditions as in Fig. 3.

ty during laser pumping we used the intercombination line $6s^2\,^1S_0$–$5d6p'\,^3D^o_1$, at $\lambda=413.24$ nm, which has an oscillator strength of $f=0.01$ (cf. Table I). The hooks of this intercombination line disappear for $\log_{10}[\bar{N}l(\text{in } m^{-2})<18.5]$. At our ground-state densities, this occurs just after the initial saturation of the resonance line along the entire vapor column, i.e., shortly after 45 ns (cf. Fig. 3). Although the ground-state density was too small to be measured directly for larger delay times, it is indicated by a dashed line; given the saturation, the ground-state density could in fact be derived from the population of the laser-pumped resonance level.

It is a remarkable feature of Fig. 3 that the population of the level $5d\,^1D_2$ follows that of the level $6p\,^1P^o_1$, the population ratio at 45 ns being that of the statistical weights. The level $5d\,^3D_2$ (cf. Fig. 4) exhibits the same behavior. As a consequence of the efficient excitation of the level $6p\,^1P^o_1$, a population inversion with these two metastable levels is built up and stimulated emission in the transitions to the levels $5d\,^3D_2$ and $5d\,^1D_2$ at 1.13 and 1.5 μm follows.[42] We observed the emission at 1.13 μm along the furnace axis in the direction of the pump laser. The infrared pulse had a length of 15 ns and we measured a

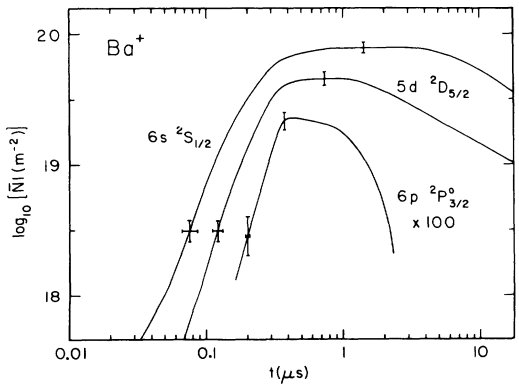

FIG. 5. Logarithmic population histories of the ground state ($6s\,^2S_{1/2}$), a metastable level ($5d\,^2D_{5/2}$), and a resonance level ($6p\,^2P^o_{3/2}$, 100× enlarged) of Ba^+. Experimental conditions as in Fig. 3.

delay of about 20 ns with respect to the beginning of the pump-laser pulse. Since these times are of the same magnitude as the absolute accuracy of our delay time measurements, we could not determine the initial inversion nor the population lag of the two metastable levels. A more detailed analysis of this point can however be given in the context of Sec. IV A 2.

We conclude from Fig. 3 that—for delay times $\gtrsim 50$ ns—there existed a homogenously excited vapor column along the optical axis and that not only the laser-excited level $6p\,^1P^o_1$, but some of the metastable levels were populated as well. We note therefore, that the starting point for further excitation processes in the alkaline-earth elements Ba, Sr, and Ca is different from that in the alkali-metals Na and Li. In the former there are low-lying metastable levels, which are speedily populated by stimulated transitions; this prevents an exclusive excitation of the resonance level as it can occur in alkali-metals.

Figure 4 shows that the two fine-structure components $J=1$ and $J=3$ of the term $5d\,^3D$ are populated at a much slower rate than the level $5d\,^3D_2$. It should be mentioned though, that for very short delays of about 5 ns, the level $5d\,^3D_3$ is populated faster than $5d\,^3D_2$, but is overtaken by the latter very rapidly afterward. This fact, which cannot be seen on Fig. 4, will be discussed in Sec. IV A 3.

Both Figs. 3 and 4 exhibit a marked minimum at 850 ns and a following rise in population of the ground state and the metastable levels for times >1 μs. This behavior is a consequence of the very efficient ionization, and of the subsequent cooling of the plasma, when recombination sets in after the end of the laser pulse.

It can also be seen from Fig. 4 that the levels of the $6p\,^3P^o$ term are populated very efficiently and with great speed—although electric dipole transitions from the laser-excited level are forbidden on parity grounds. Figure 4 furthermore confirms that the level $6p\,^3P^o_1$ is depopulated because of the near coincidence of the transition $6p\,^3P^o_1$–$6d\,^3D_1$ at 553.586 nm with the wavelength of the pump laser: The level $^3P^o_1$ is clearly underpopulated with respect to the other fine-structure levels of the $6p\,^3P^o$ term. The same level is also connected to the ground state with a relatively strong intercombination transition [37] ($6s^2\,^1S_0$–$6p\,^3P^o_1$, $\lambda=791.134$ nm, $f=0.01$) so that it is impossible to maintain a population inversion with respect to the scarcely populated ground state; this leads to the radical depopulation of $6p\,^3P^o_1$ for times 600 ns $<t<2$ μs.

As will be discussed in Sec. IV A 4 we believe that the levels of the $6p\,^3P^o$ term are populated by stimulated electronic anti-Stokes Raman scattering (SERS) from the laser-pumped $6p\,^1P^o_1$ level via virtual states near levels $6d'\,^3D_{1,2}$.[46] The level $6p\,^3P^o_2$ is appreciably populated at delay times of about 5 ns already. The nearly synchronous excitation of the level $5d\,^3D_3$ mentioned above, may therefore be attrubuted to stimulated emission in the line $5d\,^3D_3$–$6p\,^3P^o_2$ ($\lambda=2551.57$ nm).[47]

Figure 5 shows the time-dependent populations of levels belonging to Ba^+, namely, of the ground state $6s\,^2S_{1/2}$, the metastable level $5d\,^2D_{5/2}$, and the resonance level $6p\,^2P^o_{3/2}$ ($E=21\,952$ cm^{-1}). Ionization is very fast: after 330 ns, already 80% of the Ba atoms are ionized, and the maximum ionization of almost 100% is reached at about

850 ns. After the laser pulse is over, i.e., for times >1 μs, the plasma begins to cool again: the level $6p\,^2P^o_{3/2}$ decays rapidly, followed by the metastable $5d\,^2D_{5/2}$ and, slowly, by the ground state $6s\,^2S_{1/2}$. This leads to the characteristic rise that is observed beyond 1 μs for the densities of the ground and metastable levels belonging to the neutral barium atom.

Boltzmann temperatures kT_B as a function of delay time are given in Fig. 6. They are derived from the ratios $\bar{N}l(5d\,^2D_{5/2})/\bar{N}l(6s\,^2S_{1/2})$ and $\bar{N}l(6p\,^2P^o_{3/2})/\bar{N}l(6s\,^2S_{1/2})$. As long as local thermodynamic equilibrium (LTE) between these ion levels prevails, the Boltzmann temperatures corresponding to these ratios are identical and provide a means to determine the electron temperature, because then $kT_B=kT_e$. The two Boltzmann temperatures reach their respective maximum values of 0.45 ± 0.06 eV and 0.43 ± 0.02 eV at a delay of 400 ns (cf. Fig. 6). The good agreement of the two values indicates, that the assumption of LTE is justified and that the electron temperature kT_e has a maximum value of 0.44 ± 0.03 eV. (It must be emphasized, that in the errors given here and in Fig. 6 only the measuring errors are included, but not the errors of the f values.)

The electron density $\bar{N}_e$ plotted in Fig. 6 is in fact the sum over the population densities of the $6s$ and $5d$ configurations of Ba^+; contributions from the configuration $6p$ are negligible. The population of the ion level $5d\,^2D_{3/2}$ which had not been measured, was calculated with the aid of the electron temperature and was included in the determination of the total ion density. The resulting maximum ionization exceeds 100%; this is however, compatible with our measuring errors and with the uncertainty in the f values.[48]

A more exact estimate of the maximum degree of ionization can be obtained from the minimum in the populations of neutral barium at about 850 ns. This yields an ionization of about 98 ± 1%, and such an ionization requires an electron temperature of 0.45 ± 0.02 eV according to the Saha equation. We note that the agreement of the electron temperatures of the ionization and excitation equilibria provides a further confirmation for the assumption of LTE.

A more detailed discussion on LTE between the ion levels will be given in Sec. IV C. It will be seen there, that the measured Boltzmann temperature can be set equal to the electron temperature provided the electron density exceeds 10^{20} m^{-3}, i.e., in our case, for delay times ≥ 140 ns.

We now turn to the behavior of the strontium contained in the furnace. (As the initial relative strontium concentration of ≈ 10% was diminishing while the furnace was running, the ratio between the barium and strontium densities had to be determined repeatedly.) The densities of the ground state $5s^2\,^1S_0$ and the metastable $5p\,^3P^o_2$ level of neutral Sr, which were measured during the laser pulse, are plotted vs time in Fig. 7. Figure 7 also shows the sum of the densities of the excited levels of neutral strontium and of all levels belonging to the Sr ion (denoted as Sr^*+Sr^+); this sum is in fact the difference between the strontium ground-state densities before and during laser pumping. The efficient excitation of Sr, which reaches a maximum of 80% at 1 μs is of interest, because the excitation of an atomic system that is not directly affected by the pump laser requires collisions (see also Skinner[10]).

The time behavior of the ground-state density of the Sr ion is indicated as a dashed curve in Fig. 7. This dashed curve refers to a relative scale, since the measurement of the hooks of one of the resonance lines of the Sr ion was carried out without a simultaneous reference to the ground-state density of neutral strontium. We note that the curves for (Sr^*+Sr^+) and for the Sr^+ ground state of Fig. 7 exhibit a very similar behavior for times >400 ns—in contrast to that of the level $5p\,^3P^o_2$—and assume therefore, that the combined excitation and ionization (Sr^*+Sr^+) of 80% represents mainly ionization.

In a LTE plasma, the 21 ± 4% of the Sr population that

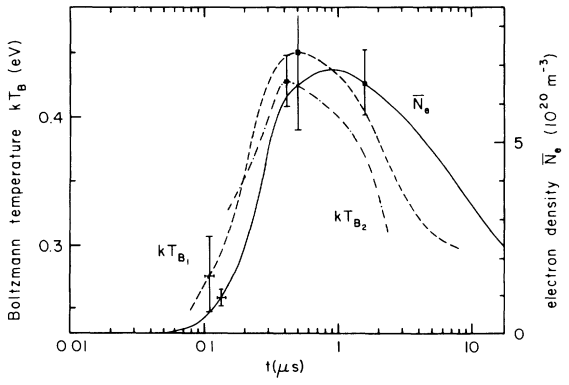

FIG. 6. Time dependence of the electron density $\bar{N}_e$ (——) derived from the sum of the densities of the Ba^+ configurations $6s$ and $5d$ and Boltzmann temperatures kT_B relating to the populations of the ground state $6s\,^2S_{1/2}$ and, respectively, the metastable and resonance levels $5d\,^2D_{5/2}$ (kT_{B_1}, — — —) and $6p\,^2P^o_{3/2}$ (kT_{B_2}, —·—·) of the Ba ion. Experimental conditions as in Fig. 3.

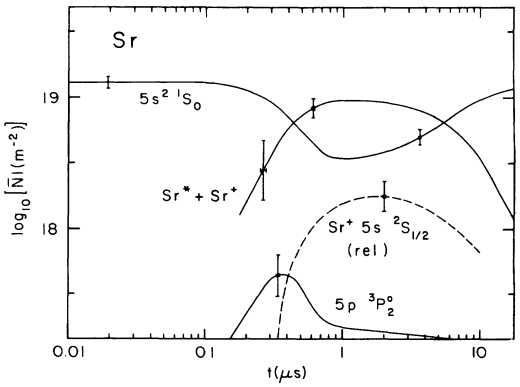

FIG. 7. Logarithmic population histories of the Sr atoms and ions that were present in the furnace as an impurity of Ba. Absolute column densities are shown for the Sr ground state ($5s^2\,^1S_0$), for a low-lying metastable level ($5p\,^3P^o_2$), and for the sum of all levels of Sr and Sr^+ except the neutral ground state (Sr^*+Sr^+). A relative density is given for the Sr^+ ground state $5s\,^2S_{1/2}$. Experimental conditions as in Fig. 3.

remain in the neutral ground state at the time of maximum excitation and ionization, and the measured electron density of 6×10^{20} m^{-3} (cf. Fig. 6) correspond to an electron temperature of 0.40±0.01 eV. The experimentally observed excitation of Sr is therefore consistent with the measured Boltzmann temperature (0.44±0.03 eV) of the Ba^+ levels.

A similar calculation based on observations of the resonance line of calcium yields and electron temperature $kT_e \leq 0.36$ eV only. No excitation could be measured here. The small concentration of about 0.2% Ca in the vapor led to large measurement uncertainties but we can assume that a 20% reduction of the Ca atoms in the ground state (corresponding to the above $kT_e \leq 0.36$ eV) could have been detected. As will be seen in Sec. IV D the small density (and thus lacking opacity in the reaonance line) may also prevent the Ca atoms from reaching LTE.

2. *A third of the full laser power (2.1 GW m^{-2}, Fig. 8)*

Figure 8 displays the time behavior of some selected[49] levels when only 30.5% (2.1 GW m^{-2}) of the full laser irradiation are used. The behavior is similar to that with the full laser power, but all processes are slower. The assumption of a homogenous excitation along the vapor column may not be given here: Saturation of the resonance transition is achieved at about 140 ns, yet the maximum population of the resonance level occurs already at 80 ns. (With full laser power, both these events took place at the same time.)

The ionizing processes are much slower. At 330 ns only 22% of the Ba atoms are ionized here, in contrast to the 80% at full laser irradiance. Nevertheless, even here the vapor is almost completely ionized shortly after the end of the laser pulse, at 1.3 μs. The degree of ionization, however, is slightly smaller than at full laser irradiance.

3. *A tenth of the full laser power (0.7 GW m^{-2}, Fig. 9)*

Figure 9 shows the time-resolved population of some selected[49] levels with the laser irradiance attenuated to 10.1% (0.7 GW m^{-2}). Saturation of the resonance transition along the vapor column is no longer established. One must assume, therefore, that large population-density gradients along the optical axis are present.

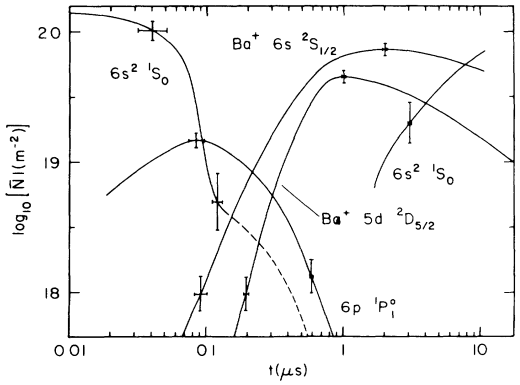

FIG. 8. Logarithmic population histories of selected Ba and Ba^+ levels. Ba density and Ar pressure were the same as those used for Figs. 3–7, but the laser energy was reduced to about one-third, viz., 2.1 GW m^{-2}.

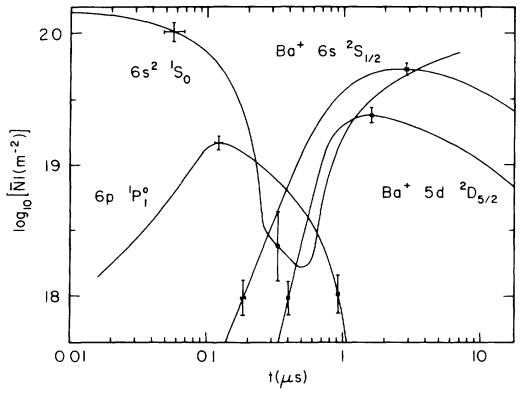

FIG. 9. Logarithmic population histories of selected Ba and Ba^+ levels. Ba density and Ar pressure were the same as those used for Figs. 3–7, but the laser energy was reduced to a tenth (0.7 GW m^{-2}) of that used for Figs. 3–7.

The degree of ionization after 330 ns is only 3.5%, nevertheless a maximum of about 66% is reached at 2 μs. Interestingly, ionization still grows after the end of the laser pulse. This behavior, which is another sign for the influence of collision processes, was also observed by Bréchignac and Cahuzac[11,12] as well as by Bachor and Kock.[13–15]

The time it takes for burning through the vapor is now comparable with or even larger than the ionization time at full laser power. Therefore the ionization in the layers of the vapor that are first excited can be complete, at a time when laser excitation in the following layers has not even started.

In the present case, the temporal behavior at a certain position along the optical axis cannot be determined uniquely by the hook measurements, since the population densities derived are averaged along the optical axis [cf. Eq. (3.1)]. For this reason, Bachor and Kock[14] had to take account of the population gradients in their model. This made their interpretation difficult.

Our observations with reduced laser irradiance show that the interpretation of the results is difficult if the time it takes the laser to burn through the vapor is larger than the characteristic times of the different plasma processes. In our experiment these difficulties were avoided only at full laser irradiance. To further investigate the influence of the laser power on the ionization efficiency, one should therefore use smaller lengths of the vapor column at the same density or larger laser irradiances. Since our laser power was restricted and the furnace length not easily variable, neither of these variants was pursued. We did, however, measure the ionization efficiency as a function of density.

4. *Higher density and full laser power (Fig. 10)*

Figure 10 presents the time behavior of some selected[49] level populations at a column density $\bar{N}l = 2.23\times10^{20}$ m^{-2} (±6%) which was 53% higher than that used for

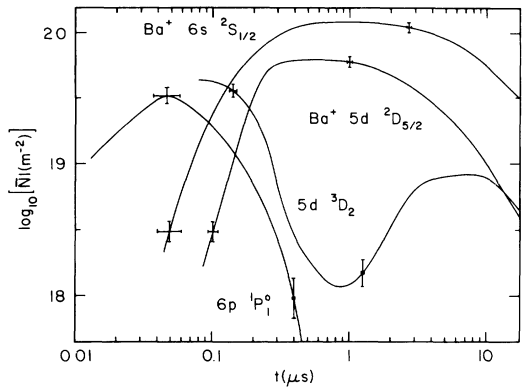

FIG. 10. Logarithmic population histories of selected Ba and Ba^+ levels with increased total Ba density ($\bar{N}_0 l = 2.23 \times 10^{20}$ m^{-2}, $\bar{N}_0 \simeq 9.7 \times 10^{20}$ m^{-3}) but with equal Ar pressure as in Figs. 3–7. The laser irradiance was 6.7 GW m^{-2} (i.e., 95% of that used for Figs. 3–7).

Figs. 3–9. The laser power was 6.7 GW m^{-2} (i.e., 95% of that used for Figs. 3–7). The ground-state density during laser pumping and the levels $5d\ ^1D_2$ and $6p\ ^3P^o_{0,1}$ were not measured here.

The behavior is similar to that with our standard density under full laser irradiance (Figs. 3-5), but ionization rises faster: after 200 ns already 57% and at 330 ns 94% of the Ba atoms in the column are ionized. The increase in ionization rate with density is an unambiguous indication that collision processes are dominant in the ionization. The minimum of the metastable states at 800 ns shows that the maximum ionization occurs at the same time as with our standard conditions.

5. *Ionization efficiency (Fig. 11)*

The ionization efficiency as a function of vapor density is shown in Fig. 11 for full laser power. The values plotted indicate the maximum of the ionization attained; the delay times at which the maximum was reached decreased with increasing density.

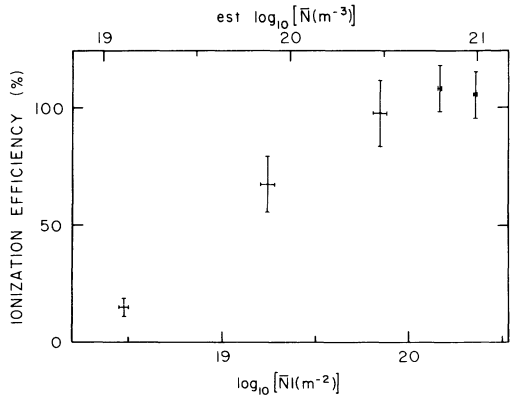

FIG. 11. Maximum ionization efficiency vs column density and approximative density (upper scale). The time needed to reach maximum ionization became shorter with increasing density. Laser irradiance and Ar pressure as in Figs. 3–7.

The pronounced rise of the efficiency with density does not support the dominant two-photon ionization suggested in the model of Bachor and Kock[14]; on the contrary, the curve of Fig. 11 points to a prominent role of the different collisional processes. The results by Skinner,[10] who has found a very similar behavior of the ionization efficiency with density, are comparable with ours if the different experimental conditions are taken into account (cf. Sec. III D).

Although the curve of Fig. 11 reveals the importance of collision processes in the ionization for the density range shown, it is still conceivable that the processes responsible for the 20% ionization at the lowest density ($\approx 10^{19}$ m^{-3}) are (i) two-photon ionization and (ii) population of high-lying levels by SERS with subsequent ionization by the laser.

B. Emission measurements

We observed the emission spectrum of the laser-excited column through the central sidearm of the furnace and measured it photoelectrically with a radiometrically calibrated 0.3-m spectrometer. For small densities ($< 5 \times 10^{19}$ m^{-3}) the emission as seen by eye is green: resonance fluorescence dominates the visual spectrum. With increasing density, however, the color of the excited vapor becomes greenish-white first, and later—at the densities normally used by us ($> 3 \times 10^{20}$ m^{-3})—white. This change of color goes along with the rising ionization efficiency shown in Fig. 11.

Detailed measurements of the emission were carried out at 4.9 GW m^{-2} (70% of the full laser irradiance) and at the density of 6.3×10^{20} m^{-3} that had also been used for taking the data shown in Figs. 3–9. The emission spectrum was that of Ba.[47,37] This implies that high-lying levels were populated with appreciable efficiency, when the density was high enough. Such a behavior is to be expected for our plasma that has an electron density of $\approx 6 \times 10^{20}$ m^{-3} and a temperature of 5000 K. In the model of Measures *et al.*[19–21]—as in most plasma models—these high-lying states are in fact needed. Apart from the resonance line, the strongest lines were those originating from the upper term of the line $6p\ ^3P^o_1 - 6d\ ^3D_1$ (that nearly coincides with the pump radiation), and the resonance lines of Ba II. In general, the emission pulses observed at the wavelengths of given Ba I and Ba II lines had rise times that ranged between 280 and 450 ns and 500 and 700 ns, respectively.

In order to derive the relative number densities ($\sim N_j/g_j$) of the emitting states, we first divided the signals by the spectral sensitivity of the detection system as well as by the transition probabilities and statistical weights g_j of, respectively, the lines observed and their upper levels. We then made a correction for optical thickness by estimating "escape factors" according to Holstein,[50,51] where needed. For simplicity we calculated these factors for cylindrical symmetry (the radius of the cylinder being approximately that of the pump laser beam in the furnace, viz., 2 mm) and for pure Doppler broadening (at a furnace temperature of 1150 K). The resulting

escape coefficients ranged between 1 and 5×10^{-3}. Uncertainties in these estimates are to be expected, since the calculations of Holstein are for a stationary, homogeneous plasma; yet our plasma is highly time-dependent and has population gradients at the edges of the plasma that are difficult to estimate. By assuming pure Doppler profiles (which enabled us to use an analytical expression for calculating the escape factors), we have also neglected resonance, Stark, saturation, and van der Waals broadening.

By comparing the population of the Ba^+ resonance level $6p\ ^2P^o_{3/2}$ that had been determined from emission with that measured by the hook method, we were able to put the relative number densities derived from our emission measurements on an absolute scale. (An absolute radiance calibration of the spectrometer was, therefore, unnecessary.)

In Fig. 12 we plotted the number densities N_j/g_j of the high-lying states as a function of their energies E_j. The values given are derived from the radiance observed at a delay of 400 ns. At that time most of the emission pulses had their maxima. For completeness, the densities of the levels of the configurations $5d$ and $6p$, which had been measured with the hook method at the same time[52] are given in Fig. 12 as well. The data points can be approximated by a straight line representing a Boltzmann temperature of 0.33 ± 0.03 eV. This indicates that the high-lying levels are in LTE with the low-lying ones (except for the $6d\ ^3D$ term, which is directly affected by the pump radiation). This confirms the assumptions of Measures *et al.*,[21] who have used LTE populations for the high-lying levels in their model. However, the Boltzmann temperature of 0.33 eV obtained from the emission measurements at 400 ns is smaller than that of 0.44 eV determined with the hook measurements (cf. Fig. 6). A possible explanation for this discrepancy is the delay caused by radiation trapping. An escape factor of 10^{-2} means, for example, that a photon emitted is on the average absorbed and reemitted 100 times before it leaves the laser-excited zone. The time dependence of the pulses therefore hardly reflects that of the populations; a delay in the peak emission is rather likely. In fact, rise times between 280 and 350 ns were observed for transitions with escape factors close to unity and for other optically thin lines (with unknown f values) connecting the two high-lying terms $6p'\ ^3F^o$ and $6d'\ ^3G$.

As will be explained in Sec. IV B 2, the maximum population of the high-lying states is to be expected to occur at the same time as the maximum of $\dot{N}_e/N_e$. At full laser irradiance this is the case at 240 ns (cf. Fig. 6), where the electron temperature is only 0.38 ± 0.03 eV. This value is already compatible with that of 0.33 ± 0.03 eV following from Fig. 12, but we recall that this latter value was taken with only 70% of the full laser irradiance. This tends to reduce the apparent difference.

If we assume an average delay of 160 ns between the emission peaks and the peak populations, a rough estimate indicates that the densities of the high-lying levels shown in Fig. 12 should be increased by a factor of 2. They then represent the actual populations at a time of 240 ns. In view of the large number of assumptions used, however, we do not expect that the densities of the high-lying states are known to within better than a factor of about 10 on an absolute scale.

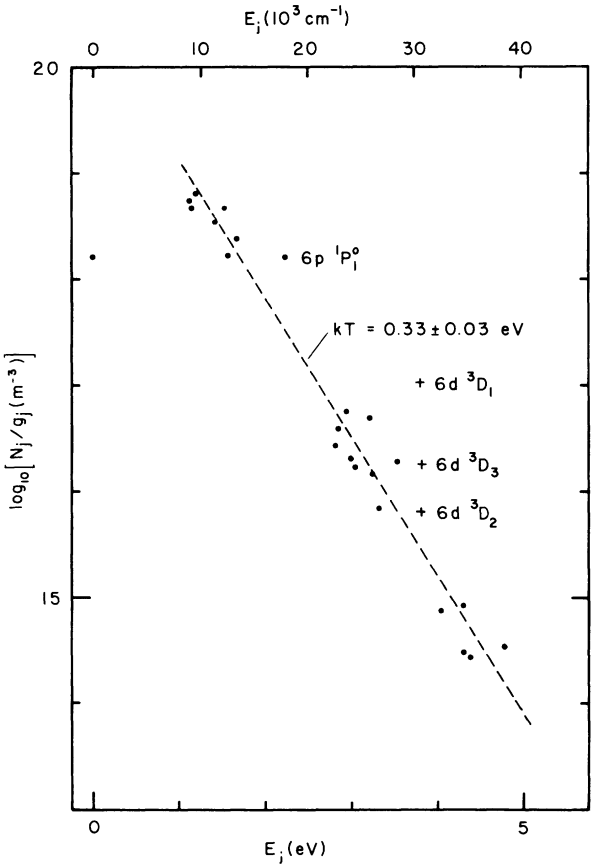

FIG. 12. Logarithmic densities of Ba states at 400 ns vs level energy. Ba density and Ar pressure as in Figs. 3–7; laser energy 4.9 GW m^{-2} (i.e., 70% of that used for Figs. 3–7). The data for $E_j \geq 2.5$ eV were obtained from emission measurements and those for $E_j < 2.5$ eV from hook spectra (see Ref. 52). The overpopulation of the laser-pumped level $6p\ ^1P^o_1$ and of the $6p\ ^3P^o$ term (which has an extra excitation channel, because the $6p\ ^3P^o_1$–$6d\ ^3D_1$ transition nearly coincides with the pump laser wavelength) is clearly seen.

Summarizing we can say, that there is a near-thermal population of the high-lying states presumably caused by electron collisions. We have looked for the effects of energy-pooling collisions, but found no evidence.[53] Measurements of optically thin lines connecting high-lying levels and of lines with escape factors close to unity indicated that the maximum populations are in fact reached between 280 and 350 ns. The foregoing arguments, however, would lead us to expect the maxima rather earlier, viz., at about 240 ns. This is reasonable if we recall that we worked only at 70% of the full laser power.

C. Additional measurements and observations

We also measured the delay of the laser beam transmitted through the furnace with respect to the part of the beam propagating along the reference arm of the interferometer. The measured delay times at the column density used for Figs. 3–9, viz., 1.46×10^{20} m^{-2}, are 16 ± 2 ns,

80 ± 10 ns, and about 180 ns with 100%, and 30%, and 10% of the full laser irradiance, respectively. These delays are only about half of the saturation times for the resonance transition determined from the hook measurements along the vapor column. The pulses were, however, not spectrally analyzed, so that it is not known whether the transmitted pulses were shifted in wavelength with respect to the incoming laser pulse. One could imagine effects like frequency broadening of the laser pulses because of self-focusing[54] or the anomalous conical emission whose wavelength was shifted with respect to the exciting laser pulse, as observed in Ba vapor by Skinner and Kleiber.[55]

Strong broadening of the level $6p\ ^1P_1^o$ was observed. For delay times >150 ns the hooks of the absorption lines out of this level are almost "devoured" by the absorption. As these absorption lines are optically thick, this means that their equivalent widths are comparable to their hook separations. Quantitively this effect can be well explained by saturation (power) broadening of the resonance line (see, e.g., Ref. 56). Saturation broadening would imply, however, that the two lines at 487.765 and 494.735 nm (both involving the $6p\ ^1P_1^o$ level, see Table I) should show the same behavior. Yet we could observe cases where the hooks were nearly "devoured" in one line only, whereas the hooks of the other line were almost unaffected. The explanation of this broadening therefore remains an open question.

D. Comparison with other experiments

The experimental conditions of Bachor and Kock[13–15] are similar to ours, with the important exception of their smaller laser irradiance (0.04—0.05 $\mathrm{GW\,m^{-2}}$). Although the smallest irradiance used in our experiment (a tenth of our full laser power, 0.7 $\mathrm{GW\,m^{-2}}$) is still larger than their irradiance by about a factor of 16, the results of the two experiments are comparable (see Fig. 9 of this paper and Fig. 3 of their latest paper[14]). Keeping in mind that our densities are based on corrected f values (cf. Table I), we conclude that—within the error limits—the maximum populations of the levels $6p\ ^3P_2^o$ and $5d\ ^1D_2$ of neutral Ba and $6s\ ^2S_{1/2}$ of Ba^+ were the same in both experiments. On the other hand, Bachor and Kock had observed a population of the laser-pumped level $6p\ ^1P_1^o$ that was twice as large as ours, and the maximum populations of the neutral Ba levels in their experiment were reached at delay times that are about twice as long as those observed by us. The larger delays can probably be explained by the slower rise time of the laser pulse in Bachor and Kock's experiment. As these authors used a Michelson interferometer, the real length of the vapor column is only half of that appearing in the dispersion measurements. For a comparable excitation they need therefore only half of our laser power. Nevertheless, a discrepancy of 1 order of magnitude in laser irradiance remains.

On the contrary, the ionization efficiency found by Skinner[10] is compatible with ours. At a Ba density of $\approx5.2\times10^{20}\ \mathrm{m^{-3}}$ and an average laser irradiance of 0.72 $\mathrm{GW\,m^{-2}}$ (6×10^{20} photons per $\mathrm{m^2}$ in 300 ns), Skinner attained a column density of $8\times10^{18}\ \mathrm{m^{-2}}$ in the Ba^+ ground state (Fig. 4 in Ref. 10), i.e., 19% of all atoms ended up in this level. In our measurements, at a Ba density of $\approx6.3\times10^{20}\ \mathrm{m^{-3}}$ and with a tenth of the full laser irradiance (0.7 $\mathrm{GW\,m^{-2}}$, 1.42×10^{21} photons per $\mathrm{m^2}$ in 750 ns) we find a maximum column density of $5.3\times10^{19}\ \mathrm{m^{-2}}$, or 36% of all atoms in the ion ground state. Given the equal laser irradiance[57] in both experiments, the slightly higher density and the longer (2.5 times) laser pulse in our experiment, our twice-as-large ionization efficiency seems to be in reasonable agreement with the results of Skinner.

In summary, the agreement of the three experiments is good, except for the discrepancy between our laser irradiance and that reported by Bachor and Kock.[14] Skinner's irradiance is expected to be the most reliable; he has measured it very carefully and gave an absolute error of less than 10%.[10]

IV. INTERPRETATION OF THE RESULTS

The results to be discussed in this section were taken with the conditions used for Figs. 3–7; namely, with a column density of $1.46\times10^{20}\ \mathrm{m^{-2}}$ and with the full laser power of 7 $\mathrm{GW\,m^{-2}}$.

A. Population of excited Ba levels

1. *Laser-pumped level $6p\ ^1P_1^o$*

The time of 40 ns it takes to reach the maximum excitation of the level $6p\ ^1P_1^o$ along the vapor column is determined by the energy input of the laser during this period. The pulse shown in Fig. 3 delivers an input of 1.7×10^{20} photons per $\mathrm{m^2}$ in these first 40 ns. An estimate of the energy balance must take into account not only the laser-pumped level $6p\ ^1P_1^o$ but all other populated low-lying levels, since these are excited via the resonance level as well, for these short delay times: There are 1.46×10^{20} excited atoms per $\mathrm{m^2}$ at 40 ns. Of the excited levels, $6p\ ^1P_1^o$ is the only one giving rise to a significant loss by spontaneous emission during the first 40 ns. Given an average column density of about $2\times10^{19}\ \mathrm{m^{-2}}$ for $6p\ ^1P_1^o$ and the transition probability,[37,36] $1.19\times10^8\ \mathrm{s^{-1}}$ for the resonance line, the loss is estimated to be 9.5×10^{19} photons per $\mathrm{m^2}$ in this time. The number of photons required for excitation and to resupply the photons lost by spontaneous emission is therefore 2.4×10^{20} photons per $\mathrm{m^2}$, in reasonable agreement with the 1.7×10^{20} photons per $\mathrm{m^2}$ delivered by the laser. It might be worthwhile mentioning that the actual pumping time of an atomic transition is much less than 1 ns for typical laser irradiances,[20] i.e., much smaller than the values given here for the saturation of the entire vapor column.

2. *Levels $5d\ ^3D_2$ and $5d\ ^1D_2$*

Within the limits of the experimentally given time resolution, the excitation of the levels $5d\ ^3D_2$ and $^1D_2$ is as fast as that of the laser-pumped level $6p\ ^1P_1^o$. However, if

one uses the observed population density of this latter level as a (nonlinear) time scale, it is possible to recognize that the density of the level $5d\,^1D_2$ follows that of the laser-pumped level $6p\,^1P_1^o$ almost without delay ($\lesssim 3$ ns), and that of $5d\,^3D_2$ has a delay of only ≈ 10 ns.

The very fast population of these two metastable levels is due to stimulated emission in the two transitions $5d\,^3D_2-6p\,^1P_1^o$ ($\lambda=1130.304$ nm) and $5d\,^1D_2-6p\,^1P_1^o$ ($\lambda=1500.04$ nm). We have observed the emission at 1.13 μm. Its pulse length was 15 ns and it occurred at about 20 ns; given the uncertainty of 10–20 ns for our delay measurement, the measured delay of 20 ns agrees with the 10-ns delay derived from the hook measurements.

A numerical estimate also shows that the inverted column density $\Delta\bar{N}l=[\bar{N}_2-(g_2/g_1)\bar{N}_1]l$ exceeds that needed for amplification. If one uses the expressions of Yariv[58] for the small signal gain γ of an inverted transition, assumes pure Doppler broadening with a rectangular line shape (width $\simeq$500 MHz at 870°C), and defines the threshold gain as $\gamma_0 l=1$ ($l=0.23$ m being the length of the heated zone and thus of the inverted vapor column) one obtains $\Delta N_{\min} l=1.1\times10^{17}$ m^{-2}. This is only about 0.5% of the maximum density measured for the level $6p\,^1P_1^o$. It might be pointed out, however, that the emission observed along the optical axis is "amplified spontaneous emission" (ASE) rather than "superfluorescence." This was verified with the aid of formulas given by Arecchi and Courtens[59] and by Bonifacio and Lugiato.[60]

3. Levels $5d\,^3D_1$ and $5d\,^3D_3$

From Fig. 4 it can be seen that the two fine-structure components $J=1$ and $J=3$ belonging to the $5d\,^3D$ term are populated more slowly that the level $J=2$, discussed under IV A 2. The most plausible population mechanisms are collisions with Ar buffer-gas atoms, fine-structure mixing collisions, and collisions with electrons (the latter though only for larger delays, where N_e is big enough). The fine-structure splittings $\Delta E_{J_1J_2}$ of the $5d\,^3D$ term, $\Delta E_{12}=0.02$ eV and $\Delta E_{23}=0.05$ eV, are smaller than the thermal energy $kT=0.1$ eV at a temperature of 870°C in the furnace. Such collisions are therefore possible. The experiment confirms that a population by collisions occurs: One observes that the fine-structure components $J=1$ and 3 are populated much faster at the higher density and both these levels show the same behavior.[35]

For very-short-delay times ($\approx$5 ns), $5d\,^3D_3$ is the level of the $5d\,^3D$ term that is populated fastest. We assume that it is populated by stimulated emission through the transition $5d\,^3D_3-6p\,^3P_2^o$ ($\lambda=2551.57$ nm). For this to occur the level $6p\,^3P_2^o$ must have a similar behavior for very-short-delay times—as observed. The f value of the 2.55-μm line is about an order of magnitude larger than those of the two infrared lines at 1.13 and 1.5 μm.[61] It should therefore be possible that the level $5d\,^3D_3$ is populated by stimulated emission, notwithstanding the fact that the inversion of the 2.55-μm transition is certainly smaller than that of the above-mentioned two 1.13- and 1.50-μm lines, whose upper level is the laser-pumped $6p\,^1P_1^o$.

4. $6p\,^3P^o$ term

The efficient population of the $6p\,^3P^o$ term—especially that of the level $6p\,^3P_2^o$—was perhaps the most surprising process observed at short delay times ($\lesssim$100 ns). A population by stimulated emission from the laser-pumped $6p\,^1P_1^o$ is not possible; both terms have the same parity. Also, collisions with electrons can be excluded, as the electron density is too small for times $\lesssim$100 ns.

There are inelastic collisions between atoms in the laser-excited $6p\,^1P_1^o$ level and other excited Ba atoms that yield two atoms in the $6p\,^3P^o$ term and that are conceivable from the point of view of energy conservation and at our temperature ($kT=0.1$ eV). Collisions with atoms in the $5d\,^3D_1$ or $5d\,^3D_2$ levels could result in two atoms in the $6p\,^3P_2^o$ level, the energy defects ΔE being only 0.008 and 0.031 eV, respectively. A collision between two atoms in $5d\,^1D_2$ could also produce atoms in $5d\,^3D_2$ and $6p\,^3P_2^o$ ($|\Delta E|=0.008$ eV). These three processes are, however, incompatible with the densities observed for very short times ($\approx$5 ns); only the four levels $6p\,^1P_1^o$, $5d\,^1D_2$, $5d\,^3D_3$, and $6p\,^3P_2^o$ are appreciably populated so that only one of the needed partners ($6p\,^1P_1^o$) would be present at that time.

A fourth collisional process $5d\,^1D_2+5d\,^1D_2\rightarrow 5d\,^3D_3+6p\,^3P_2^o$ with $|\Delta E|=0.040$ eV would be possible nevertheless, but it would require an impossibly large collision cross section. For times $\lesssim$80 ns and with the aid of the corresponding differential equation, $d/dt[N(6p\,^3P_2^o)]=\bar{v}\sigma N^2(5d\,^1D_2)$, we derive a lower bound of $\sigma=3.6\times10^{-17}$ m^2 for the needed cross section, given the slope of the level density for $6p\,^3P_2^o$ in Fig. 4 and the maximum density of $5d\,^1D_2$ in Fig. 3, as well as an average relative speed $\bar{v}=6\times10^2$ m s^{-1} for the Ba atoms at the furnace temperature of 870°C. As there are no known cross sections of such collisions in Ba, we might compare this lower bound with similar "energy-pooling" collisions in Na (Refs. 18 and 62) and Cs,[63] that have cross sections between 10^{-21} and 10^{-19} m^2, and 2×10^{-19} m^2, respectively. Even the largest of these cross sections is still more than an order of magnitude smaller than the one needed by us. And an estimate of the cross section as $\sigma=\pi r^2$, with r being the radius of the atom in the relevant Ba level (0.4 nm), yields a value of only 5×10^{-19} m^2, which is two orders of magnitude smaller than that required.

A remaining possibility to explain the observed efficient population of the $6p\,^3P^o$ term is stimulated electronic anti-Stokes Raman scattering (SERS) from the laser-pumped level $6p\,^1P_1^o$ to the $6p\,^3P^o$ term via the term $6d'\,^3D$. The two levels $5d6d'\,^3D_{1,2}$ can enhance the effect as they serve as quasiresonant intermediate levels.

Carlsten and Dunn[64] have observed the Raman transitions $6s^2\,^1S_0-5d\,^3D_{1,2}$ (via $6p\,^3P_1^o$ as quasiresonant intermediate level) in Ba. Despite the small f values (of the order of 0.01) of the transitions involved, they found a maximum photon conversion efficiency of 40% and a tunable range of ±70 cm^{-1}. In our case, the energy differences between the levels $6p\,^1P_1^o$ and $6d'\,^3D_{1,2}$ are 187 cm^{-1} smaller and 80 cm^{-1} larger, respectively, than the energy of a laser photon. From the level $6p\,^1P_1^o$ only the transi-

tion $6p\,^1P_1^o-6d'\,^3D_1$($\lambda=559.33$ nm) is known,[47] but the line to the level $6d'\,^3D_2$ should be of comparable strength. Of the multiplet $6p\,^3P^o-6d'\,^3D$ there are five known lines[47,37] having f values of the order of 0.03. The population of the $6p\,^3P^o$ term by SERS thus seems to be the most likely process. The strong stray light from the pump laser in the spectrograph, however, prevented an experimental confirmation of this process.

B. Ionization of barium

Different authors have presented quite diverging opinions regarding the dominant ionization mechanism. Yet the most recent and most complete investigations of ionization by resonant laser excitation[18,7,8,11,12] agree on the importance of superelastic collisions for densities exceeding 10^{20} m^{-3}: Good results were obtained with the model of Measures.[19–21]

A discussion on whether the seed processes can also lead to the observed, efficient ionization, is complicated in Ba by the lack of the relevant cross sections. Moreover, our data do not offer much guidance on the seed processes themselves because the hook method, which was primarily used for diagnostics, is insensitive at the column densities where seed processes are expected to be dominant ($N\lesssim 10^{19}$ m^{-3}).

Here we restrict the discussion of these processes to a few remarks. A more extended discussion is given in the review of Lucatorto and McIlrath,[18] which dealt with the pertinent processes in alkali-metals.

Population of high-lying states by energy-pooling collisions ($X^*+X^*\rightarrow X^{**}+X\pm\Delta E$) with subsequent photoionization seems to be insignificant. While analyzing the emission, we could not find any pronounced selective excitation of high-lying levels, and concluded that excitation by electron collisions is dominant. In addition, we have found (cf. Sec. IV A 4), that the estimated cross sections for energy-pooling collisions ($\approx 5\times 10^{-19}$ m^2) are much too small to explain the observed excitation and efficient ionization.

We also expect associative ionization to be unimportant in Ba. The relevant cross sections are probably of the same order of magnitude as in the alkali-metals.[18,65]

Processes like energy-pooling collisions as well as associative and Penning ionization would be compatible with the (nonlinear) characteristics of the measured ionization efficiency (Fig. 11): Their rates have a quadratic density dependence. There are, however, no cross-section measurements at all of associative, Penning, nor of dimer ionization in Ba. Use of the cross sections for Penning ionization of highly-excited levels in Rb (Ref. 65) ($\approx 5\times 10^{-17}$ m^2) does not yield any appreciable contribution to the ionization.

On the other hand, a dominant two-photon ionization out of an excited level or excitation of high-lying levels by stimulated electronic Raman scattering (as the excitation process proposed for the $6p\,^3P^o$ term discussed in Sec. IV A 4) can be excluded, since their efficiency does not depend on density. At small densities ($\lesssim 10^{19}$ m^{-3})—and at larger densities during the seed phase—these two processes can, however, be dominant, as all other mechanisms are then negligible. The ionization efficiency of 15% measured at a density of 1.3×10^{19} m^{-3} (cf. Fig. 11) is best explained by these two processes.

At the usual conditions of our experiment—$\bar{N}l=1.46\times 10^{20}$ m^{-2} and full laser irradiance—the ionization is below 1% for delay times $\lesssim 40$ ns. Because of the uncertain description of the seed phase we restrict ourselves in the following to delay times greater than 40 ns, and we will discuss mainly the efficient ionization for times greater than 40 ns.

1. Superelastic electron collisions with excited Ba atoms

The relation between the cross sections Q_{ik} (m^2) for inelastic and superelastic electron collisions is derived by use of the principle of detailed balancing, and the corresponding rate coefficients K_{ik} (m^{3}s^{-1}) are then obtained by averaging $v_eQ_{ik}(v_e)$—i.e., the electron velocity times the cross section—over the velocity distribution of the electron gas (cf. Ref. 66, for example).

The connection between the rate coefficients for superelastic and inelastic collisions for Maxwellian distributions is given by[66]

$$K_{21}=\left[\frac{g_1}{g_2}\right]\exp(\epsilon_{21}/kT_e)K_{12}\ , \tag{4.1}$$

where ϵ_{21} denotes the energy difference of the transition. Consequently the collision rates $R_{ik}=N_eN_iK_k$(s^{-1}) with N_e being the electron density, are symmetrical in thermodynamic equilibrium: $R_{12}=R_{21}$.

For a laser-pumped, saturated transition however, the ratio of the number densities of the two concerned levels is $N_2/N_1=g_2/g_1$; the ratio of the corresponding collision rates is then $R_{21}/R_{12}=\exp(\epsilon_{21}/kT_e)\geq 1$, i.e., there are more superelastic than inelastic collisions. As a consequence the colliding electrons gain energy. And this energy gain of the electron gas is described by

$$\begin{aligned}\frac{d}{dt}(N_e\tfrac{3}{2}kT_e)&=\epsilon_{21}(R_{21}-R_{12})\\&=N_eN_1K_{12}\epsilon_{21}[\exp(\epsilon_{21}/kT_e)-1]\ .\end{aligned} \tag{4.2}$$

For calculating the rate coefficients we used the empirical representation of electron excitation cross sections for allowed transitions of neutral atoms, according to Drawin (see Ref. 66, for example). In his representation, the cross sections are proportional to f_{ik}/ϵ_{ki}^2, i.e., to the oscillator strength f_{ik} of the transition divided by the square of the energy difference ϵ_{ki}^2, and grow linearly at threshold. The threshold slopes Q'_{ik} are therefore proportional to f_{ik}/ϵ_{ki}^3 and the magnitude of the cross sections can be characterized by its maximum value $Q_{\max}$ or by its threshold slope Q'. The threshold slopes of two different cross sections are related by

$$\frac{Q'_{12}}{Q'_{34}}=\left[\frac{\epsilon_{43}}{\epsilon_{21}}\right]^3\frac{f_{12}}{f_{34}}\ . \tag{4.3}$$

This ratio can be used to calculate unknown cross sections from experimentally determined ones.

As long as $kT_e \ll \epsilon_{21}$ the Maxwellian distribution overlaps practically only with the linear part of the cross section and the corresponding rate coefficient can be given in the analytical approximation[67]

$$K_{12}=\left[\frac{8kT_e}{\pi m_e}\right]^{1/2} Q'_{12}(\epsilon_{21}+2kT_e)\exp\left[-\frac{\epsilon_{21}}{kT_e}\right], \qquad (4.4)$$

where m_e denotes the electron mass.

Cross sections of the Ba resonance line have been measured by Chen and Gallagher[68]; they give an error of $\pm 5\%$. From these values we derived a slope $Q'_{12}=1.5\times 10^{-19}\ \mathrm{m^2 eV^{-1}}$.

Since experimental values $\bar{N}_1(t)$ $(6s^2\,{}^1S_0)$, $\bar{N}_2(t)$ $(6p\,{}^1P_1^o)$, $\bar{N}_e(t)$, and $kT_e(t)$ are known for times ≥ 40 ns (cf. Figs. 3 and 6), we can calculate the energy density gained by the electrons through superelastic collisions with atoms in the laser-excited level $6p\,{}^1P_1^o$ in the time interval between 40 ns and t:

$$\rho_\epsilon(t)=\frac{g_1}{g_2}\epsilon_{21}\int_{40\,\mathrm{ns}}^{t} K_{12}[\exp(\epsilon_{21}/kT_e)-1]N_2N_e\,dt'\,. \qquad (4.5)$$

For times <40 ns the assumption of a Maxwellian distribution would not be justified,[18] and this would complicate the calculations appreciably. Fortunately, however, up to 40 ns the ionization is smaller than 1% ($\bar{N}_e \lesssim 6\times 10^{18}\ \mathrm{m^{-3}}$, cf. Fig. 6) and the energy gained by superelastic collisions is therefore negligible.

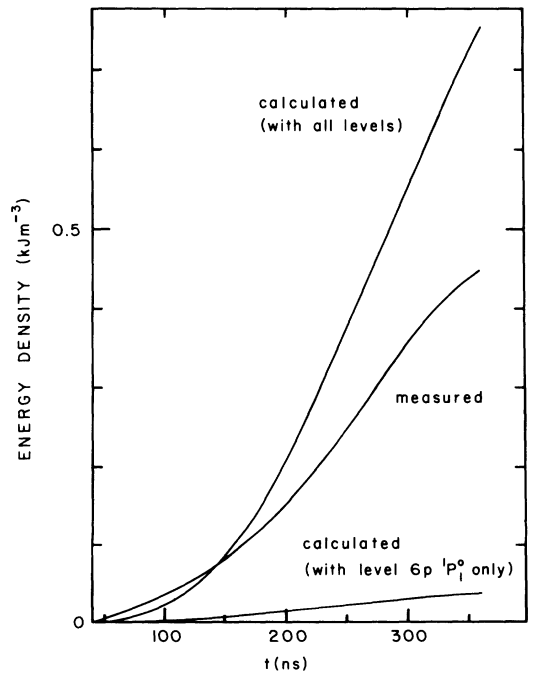

FIG. 13. Energy density in excitation, ionization, and electron motion, gained after 40 ns.

In Fig. 13 the time-dependent energy-density $\rho_\epsilon(t)$ calculated according to Eq. (4.5) is compared with the sum of the potential-energy density of the Ba atoms and ions and of the experimentally determined kinetic-energy density $\frac{3}{2}N_ekT_e$ of the electrons. The measured energy is about a factor of 10 larger than the calculated one.

As indicated in Fig. 13, the discrepancy can be reduced by taking into account superelastic collisions of all other low-lying levels ($5d\,{}^3D_{1,2,3}$, $5d\,{}^1D_2$, $6p\,{}^3P_{0,1,2}^o$), which correspond to optically forbidden transitions with the ground state. Experimental cross sections for these Ba transitions do not exist, but estimates are possible, if we assume that these cross sections are of the same order of magnitude as that for the resonance transition.

The proportionality with the f values of Eq. (4.3) is no more valid here. In the homolog case of He, for example, the cross sections for the strongly forbidden transitions $1\,{}^1S-2\,{}^1S$, $2\,{}^3S$, $2\,{}^3P$ are comparable to the cross section of the resonance transition $1\,{}^1S-2\,{}^1P$. Cross sections of these forbidden transitions in He rise much faster at threshold (5–15 times) but reach their maximum earlier, and have smaller maxima (3–10 times) than the resonance transition $1\,{}^1S-2\,{}^1P$ ($\lambda=58.4$ nm).[69,70] The assumption of appreciable cross sections for optically forbidden transitions in alkaline-earth elements is also supported by direct evidence for the corresponding collisions in laser-excited Sr (Refs. 11 and 12) and Ba.[25] In Ba we calculated the slopes of the cross sections at threshold Q'_{1k} from that of the resonance transition Q'_{res} with $Q'_{1k}/Q'_{\mathrm{res}}=(\epsilon_{\mathrm{res}}/\epsilon_{k1})^3$, i.e., we used formula (4.3) without considering the ratio of the oscillator strengths.

Since $kT_e \ll \epsilon_{k1}$ does not hold rigidly for these transitions, the approximation (4.4) is no longer valid; the rate coefficients must be evaluated numerically. For the same reason the magnitude of the maxima of the cross sections will have some influence on the rate coefficients. For lack of a more convenient representation, however, we use the one for allowed transitions by Drawin, keeping in mind that this representation yields maxima for the cross sections, and rate coefficients that are both too big for the forbidden transitions in the present case.

To calculate the more realistic energy density of Fig. 13 with Eq. (4.5), we allowed for transitions between the levels $5d\,{}^3D_{1,2,3}$, $5d\,{}^1D_2$, $6p\,{}^3P_{0,1,2}^o$, as well as between $6p\,{}^1P_1^o$ and the ground state. The resulting energy densities are almost twice as large as the measured ones. This was to be expected, since the cross sections of the forbidden transitions have in reality an energy dependence that is somewhat different from the one assumed by us. The salient point is, however, that our calculations give the correct time behavior and especially that they show the strong rise between 200 and 300 ns. This time behavior is a consequence of the superelastic collisions. If energy-pooling collisions or associative ionization prevailed, the strong rise of the ionization were to be expected earlier; their relevant rates are proportional to N^{*2}, i.e., to the square of the density of the excited states. The measurements, however, agree with our calculations, which are based on rates that are proportional to N^*N_e. And this confirms the dominance of superelastic collisions.

2. Ionization mechanism

So far we have compared only the time dependence of the *energy density* in our Ba vapor with that calculated with superelastic collisions. In the following we will show that the observed *ionization time* can be explained with a dominant electron-impact ionization.

For the electron-impact ionization cross section Q_{ic} we use the representation of Drawin,[71,66] which is very similar to the one used in Sec. IV B 1 for electron-impact excitation. The ionization cross sections Q_{ic} are proportional to the number of equivalent electrons ζ_i of level i, rather than to the oscillator strength of the pertinent transition as is the case for excitation cross sections.

The measurements of the ionization cross sections by Okuno[72] and by Dettmann and Karstensen[73] agree well for small electron energies, leading to a threshold slope $Q'_{1c}=4.5\times10^{-20}$ m^{2}eV^{-1} for the transition Ba $6s^2\,{}^1S_0 \rightarrow$ Ba$^+$ $6s\,{}^2S_{1/2}$. As only this cross section out of the Ba ground state has been measured, we estimated the cross sections for transitions out of excited Ba levels with Eq. (4.3) by replacing the oscillator strengths and the excitation energies by the number of equivalent electrons and the ionization energies, respectively.

The growth of the electron density (neglecting ion recombination and photoionization by the pump laser) is given by

$$\dot{N}_e \simeq N_e \sum_i N_i K_{ic} \ . \tag{4.6}$$

We evaluated this sum at a delay of 240 ns, where the measured $\dot{\bar{N}}_e / \bar{N}_e$ is at a maximum (cf. Fig. 6). At 240 ns the measured values are $\bar{N}_e=3.1\times10^{20}$ m^{-3}, $\dot{\bar{N}}_e=2.5\times10^{27}$ m^{-3}s^{-1}, $kT_e=0.38$ eV. To calculate the ionization rate coefficients we also took into account the lowering of the ionization energy by $\Delta\epsilon_c$ (cf. Ref. 74, for example): For our experimental conditions at a delay of 240 ns, $\Delta\epsilon_c=0.047$ eV, so that the effective ionization potential is $\epsilon'_{c1}=5.163$ eV.

If the sum in Eq. (4.6) is taken over the nine low-lying levels belonging to the configurations $6s^2$, $6s5d$, and $6s6p$, we obtain a growth of the electron density of $\dot{N}_e(240\text{ ns}) \simeq 1.1\times10^{24}$ m^{-3}s^{-1}. This value is more than 3 orders of magnitude smaller than the measured one.

This discrepancy is reduced dramatically, if one assumes that the higher-lying levels are in LTE with the lower-lying ones,[21] Eq. (4.6) then yields 10–70% of the observed growth of the ionization. In analyzing the emission (Fig. 12) we did in fact observe LTE for these levels. (Estimated relaxation times for LTE at a delay of 240 ns lie between 15 and 60 ns, if the electron-impact cross sections[75] for the transitions $5d\,{}^1D_2-6p'\,{}^1F^o_3$, $5d\,{}^3D_1-6p'\,{}^1D^o_2$, and $5d\,{}^1D_2-4f\,{}^1F^o_3$ are used; these cross sections are the only ones available for transitions between excited levels. Realistically, these relaxation times may well be shorter than 10 ns, if one considers transitions which have no measured cross sections but smaller energy gaps, as, for example, the transitions from the laser-pumped level $6p\,{}^1P^o_1$ to the configurations $5d^2$ and $6p'$. Excitation of high-lying levels in a kind of "ladder climbing" can therefore be very fast and effective and quickly lead to LTE.) If we consider in Eq. (4.6) all the levels up to 4.6 eV (i.e., $\approx$0.6 eV below the ionization limit, cf. Fig. 2) we obtain $\dot{N}_e(240\text{ ns}) = 2.6\times10^{26}$ m^{-3}s^{-1} or 1.7×10^{27} m^{-3}s^{-1}, depending on whether the high-lying levels are considered to be in equilibrium with the averaged density of the configurations $5d$ and $6p$ or with the level $6p\,{}^1P^o_1$ alone. [The level $6p\,{}^1P^o_1$ is actually overpopulated with respect to the other low-lying levels (see, e.g., Fig. 12).]

In these calculations the choice of the high-lying levels is critical, because the main contributors to the ionization rate are high-lying configurations with large statistical weights; the configuration $6d'(\langle\epsilon_{ci}\rangle=0.62$ eV, $g_{\text{tot}}=100)$, e.g., contributed 40% to the foregoing results. In our representation, ionization rate coefficients K_{ic} of very high levels, where $kT_e \gg \epsilon'_{ci}$, behave as $K_{ic}\sim(\epsilon'_{ci})^{-1}$. Thus, by summing over high enough levels in Eq. (4.6) one can obtain almost unlimited ionization rates.

Ion recombination, which has been neglected so far, will introduce some of the needed constraints. It is a well-known fact that high-lying Rydberg states are in equilibrium with the free electrons (Saha equilibrium) rather than with the low-lying levels (see Ref. 66, for example), because recombination strongly influences their population densities. Instead of Eq. (4.6) one must therefore use the complete rate equations[66,20] for all level populations and the electron density. (Simultaneously we include radiative rates and photoionization by the pump laser.) Therefore

$$\begin{aligned}\dot{N}_i = {} & N_e\left[\sum_{k(\neq i)} N_k K_{ki} - N_i \sum_{k(\neq i)} K_{ik}\right] \\ & - N_i \sum_{k(<i)} \beta_{ik} A_{ik} + \sum_{k(>i)} N_k \beta_{ki} A_{ki} \\ & - N_e N_i K_{ic} + N_e^2 N_1^+ K_{ci} - N_i \sigma_{ic} F \ (\text{for } i \geq i^*)\end{aligned} \tag{4.7}$$

$$\dot{N}_e = N_e \sum_k (N_k K_{kc} - N_e N_1^+ K_{ck}) + \sum_{k(\geq k^*)} N_k \sigma_{kc} F \ , \tag{4.8}$$

where A_{ik}(s^{-1}) denotes the rates of spontaneous emission, β_{ik} the corresponding Holstein escape factors[50,51] (cf. Sec. III B), σ_{ic}(m^2) the cross section for photoionization by the pump laser [which is possible for levels $i \geq i^*$, fulfilling the energy condition $\epsilon_i \geq$ (2.97 eV$-\Delta\epsilon_c$)], F (photons per m^{2}s^{-1}) the pump laser photon-flux, and N_1^+ the population density of the ion ground state. Since the total number of heavy particles does not change, $\dot{N}_e + \sum_i \dot{N}_i = 0$, one of the rate equations for $\dot{N}_i$ or that for $\dot{N}_e$ is redundant.

Qualitatively, we expect the following behavior of the level populations: Levels of moderate excitation ($\epsilon_i \lesssim 4$ eV) are in equilibrium with the low-lying levels; the more one approaches the ionization limit, however, the more the populations will deviate from this equilibrium, finally—at the ionization limit—they will coincide with the Saha value. Since ionization rates out of the Rydberg levels are very large, the ionization is rather sensitive to their exact population densities. In order to quantitatively investigate the influence of the various parameters, we solved Eqs. (4.7) and (4.8) numerically.

For this purpose we assumed a simplified Ba term scheme. Up to an energy of about 4.61 eV we considered all configurations, i.e., all the configurations shown in Fig. 2 except for $5f,8s',9s$. The nine low-lying levels, whose densities have been determined with the hook method, were treated as single levels. The levels of the configurations lying higher than the configuration $6s6p$ were lumped together into one "level" having the energy of the center of gravity and the total statistical weight of the configuration. For "levels" lying higher than 4.61 eV we used exact hydrogen energies $\epsilon_n=\epsilon_{c1}-R_{\rm Ba}/n^2$ with $R_{\rm Ba}$ and ϵ_{c1} being the Rydberg constant and ionization energy of Ba and with the principal quantum number n running from 5 to 16 (level 16 lying 0.005 eV below the reduced ionization limit); the statistical weight of these levels was $g_{\rm tot}=4n^2$. To approximately allow for the quantum defects of the different configurations we assumed that the level with $n=5$, for example, comprised the configurations: $9s,9p,8d,5f,5g$; the level with $n=6$: $10s,10p,9d,6f,6g,6h$, and so on.

All possible combinations of these levels were considered to be allowed transitions. The radiative lifetimes τ_i of these levels were calculated by $\tau_i=(n_i^*)^3/\gamma$ with n_i^* being the effective quantum number of level i. The decay constant $\gamma=2\times10^9$ s^{-1} was a compromise of experimentally determined decay constants for the series $6sns\ ^1S_0$ and $6snd\ ^1D_2$, $^3D_2$.[76,77] The rates of spontaneous emission A_{ik} were calculated from the radiative lifetimes by using hydrogenic branching ratios, i.e., $A_{ik}\sim[n_i^*n_k^*(n_i^{*2}-n_k^{*2})]^{-1}$.[66] From the radiative rates A_{ik}, the corresponding oscillator strengths f_{ki} could be calculated and used for determining the excitation cross sections with the formulas of Drawin (see Ref. 66, for example).[78] The photoionization cross section of the $5d\ ^3D$ term is the only experimentally determined cross section out of an excited level, and has a threshold value (at 303 nm) of $(1.8\pm0.4)\times10^{-21}$ m^2.[79] For the photoionization by the pump laser we therefore chose a constant value of 10^{-21} m^2 for the cross section σ_{ic}. (This is probably an upper bound.)

A numerical solution of the system of rate equations (4.7) and (4.8) is rather difficult, since the rates belonging to Rydberg levels are very large (i.e., of the order of 10^{12} s^{-1}). If one forgoes the calculation of the temporal development of the population densities and restricts oneself to a computation of the populations at a given time, and if one regards Eq. (4.8) for the electron density as redundant, the system of differential equations (4.7) is reduced to a system of linear equations with the electron density as a parameter. Given the electron density N_e and the derivatives $\dot{N}_i$ of all levels, one obtains the population densities N_i as a result.

Again we chose the delay time of 240 ns (where $\dot{\bar{N}}_e/\bar{N}_e$ goes through a maximum) to calculate the stationary solutions of Eq. (4.7) with our simplified atomic model. The derivatives $\dot{\bar{N}}_i$ (240 ns) of the nine levels of the configurations $6s^2$, $5d$, and $6p$ could be read off the slopes of the measured population densities $\bar{N}_i(t)$ (Figs. 3 and 4); the absolute value of the sum of the derivatives is equal to the measured $\dot{\bar{N}}_e(240\ {\rm ns})=2.5\times10^{27}$ m^{-3}s^{-1} within the experimental errors. For the remaining levels we put $\dot{N}_i=0$. The assumption of $\dot{N}_i=0$ for the higher-lying levels, a common ansatz,[66] is a good approximation, if the corresponding relaxation times τ_i are markedly shorter than the relaxation time τ_e of the ionization. Using the formulas of Mitchner and Kruger[66] for τ_i/τ_e and the densities N_i calculated with our model, we get values $\tau_i/\tau_e\leq0.02$ that justify the assumption $\dot{N}_i=0$ for the higher-lying levels. To simulate the saturation of the resonance line and the concomitant, experimentally observed overpopulation of the resonance level $6p\ ^1P_1^o$, it was sufficient to use very large values for the corresponding rates. The exact population densities were obtained by iteration, starting with the optically thin case with all Holstein escape factors[50,51] $\beta_{ik}=1$; the latter were again calculated by assuming pure Doppler profiles and cylindrical geometry with a radius of 2 mm as in Sec. III B.

Figure 14 shows the population densities obtained in this way. For comparison, the values according to the Saha equation, i.e., for equilibrium are also shown in Fig. 14. The actual results of our model calculations are the populations of the nine low-lying levels, which have also

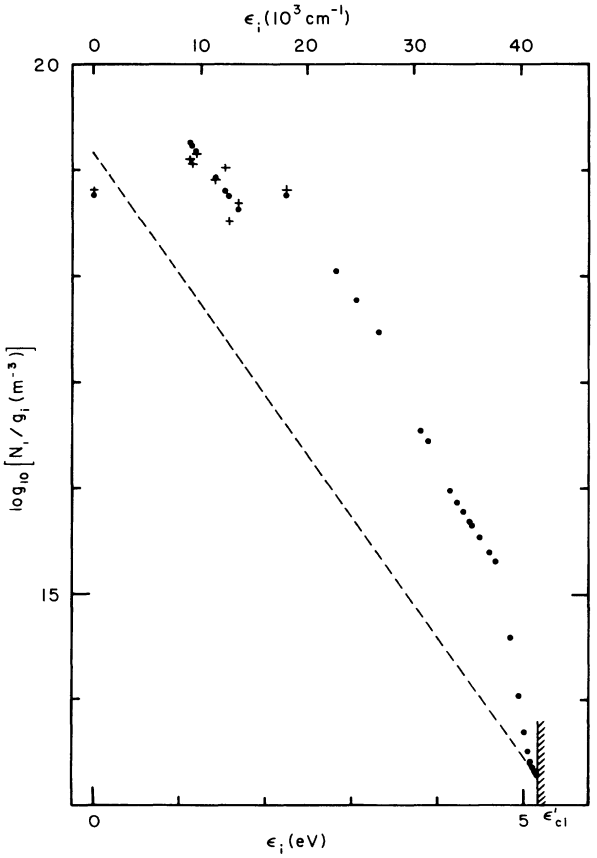

FIG. 14. Population densities at 240 ns as observed by the hook method (+) and as calculated (●) according to our model by use of rate equations. Populations corresponding to an equilibrium between ionization and recombination (Saha equilibrium) are marked by a dashed line.

been measured with the hook method. The growth of the electron density $\dot{N}_e$ however, is automatically correct, since we have used the measured value $\dot{\bar{N}}_i$ for these levels, for which $\sum_i \dot{\bar{N}}_i = -\dot{\bar{N}}_e$ is fulfilled. The agreement of the calculated and measured populations of the nine low-lying levels is excellent and the calculated total density of neutral Ba (4.6×10^{20} m^{-3}), is in reasonable agreement with the measured value (3.2×10^{20} m^{-3}) at 240 ns.

The uncertainties of the measured values that were used as parameters in the model—$kT_e = 0.38\pm0.025$ eV, $\bar{N}_e = (3.1\pm0.6)\times10^{20}$ m^{-3}, $\dot{\bar{N}}_e = (2.5\pm0.5)\times10^{27}$ m^{-3}s^{-1} (cf. Fig. 6)—result in an uncertainty of about a factor of 2 in the calculated total neutral density. The population of the laser-pumped level $6p\ ^1P_1^o$ turns out to be the most important for the ionization speed; this level lies nearest to the next-higher configurations [viz., $5d^2$ and $5d6p'$ (cf. Fig. 2)]. Consequently, the total neutral density is not a very good measure for the accuracy of our model, because the neutral density is mainly determined by the populations of the other eight low-lying levels. These populations are quite sensitive to the cross sections assumed for the transitions among them. On the other hand, the eight lowest levels do not influence the ionization speed as much as does the population of the laser-pumped level $6p\ ^1P_1^o$.

Interesting information about the behavior of the system is obtained by varying parameters as the excitation, ionization, and photoionization cross sections. Changing all excitation cross sections by a factor of 2 results in a variation of the total neutral density by almost the same factor; doing the same for the ionization cross sections changes the result by only 5%, however. This is not very surprising: The ionization speed is determined by the excitation, in particular by the transitions $6p(^1P_1^o)$–$5d^2$ and $6p(^1P_1^o)$–$5d6p'$, while the ionization rates out of Rydberg levels, for example, are amply sufficient to cope with the excitation provided. If we neglect photoionization by the laser, the calculated neutral densities will rise by about 45%; neglecting electron-impact ionization, on the other hand, will enhance these densities by more than a factor of 2.

The influence of the overpopulation of the $6d\ ^3D$ term caused by the near coincidence of the line $6p\ ^3P_1^o$–$6d\ ^3D_1$ with the pump laser (cf. Sec. III A 1)—an effect that has not been included in the present model calculations—is difficult to determine. As this line is only pumped by the laser in the far wing, the excitation efficiency is very sensitive to spectral impurities of the laser output or possible frequency shifts of the laser radiation by self-focusing (cf. Sec. III C). Figure 12 demonstrates, however, that the overpopulation of the $6d\ ^3D$ term does not influence very much the populations of nearby configurations. The additional contribution of this term to the ionization may therefore be estimated to be smaller than 10%.

Another point worth discussing is the assumption of a Maxwellian distribution of the electron velocities. The populations of the nine low-lying levels are far from being in equilibrium with the electron gas; they are mainly determined by the interaction with the pump laser. The Boltzmann temperature relating to the laser-pumped level $6p\ ^1P_1^o$ and the ground state is almost infinite; that of the metastables may even be negative. As a consequence, the high-energy tail of the Maxwellian distribution may be appreciably enhanced.[80,66,81] This would result in a sensitive increase of the excitation and ionization rates. On the other hand, collisional transitions between highly excited states may be quite efficient in smearing out this effect.[82] If the electron-velocity distribution is strongly non-Maxwellian we should in principle have observed quite different population temperatures of the excited ion configurations $5d$ and $6p$, in view of their rather different excitation energies. Figure 6 shows, however, a very good agreement between these two temperatures, suggesting that the effect may be negligible. In other words, there are enough inelastic electron collisions with atoms in levels not influenced by the pump laser; in particular with the strongly populated ion levels. This problem may be worth pursuing more carefully in the future; but it is far from simple, as the rate equations have to be solved simultaneously with the Boltzmann equation for the electron distribution function.

Summarizing we can say that the observed ionization cannot be explained by electron-impact ionization of the low-lying configurations $6s^2, 6s5d, 6s6p$ only. A dominant electron-impact ionization is possible, however, if one considers the high-lying levels as well. The small energy gaps in Ba then make possible a fast and efficient near-LTE population of these high-lying levels by a kind of "ladder climbing." [Emission measurements (cf. Sec. III B) confirm such a LTE population.] This could be an explanation for the faster ionization in Ba compared to the alkali-metals[1,2,20]: In spite of the moderate Ba density used, fast ionization was observed. Electron-impact ionization seems to dominate photoionization by the laser, yet no definite statement can be made as measurements of the relevant cross sections are lacking. We recall, however, that the ionization speed is largely determined by the excitation cross sections.

C. Population of the excited Ba^+ levels

In the preceding discussions, we have relied on the electron temperature being equal to the Boltzmann temperatures that are derived from the measured population ratios $\bar{N}(5d\ ^2D_{5/2})/\bar{N}(6s\ ^2S_{1/2})$ and $\bar{N}(6p\ ^2P^o_{3/2})/\bar{N}(6s\ ^2S_{1/2})$ of low-lying Ba^+ levels (Fig. 6). Although these two Boltzmann temperatures (kT_{6s5d} and kT_{6s6p}) agree from the time (140 ns) when the pertinent level densities can be reliably determined, it remains to be established that they represent the electron temperature kT_e as well.

Again we used numerical model calculations to investigate the relaxation times for equilibrium. Similarly to the procedure chosen in the last section, we treated the three lowest terms of Ba^+—$6s\ ^2S$, $5d\ ^2D$, and $6p\ ^2P^o$—as a three-level system (with appropriate averaged energies and statistical weights). Transition probabilities[37] and electron-excitation cross sections[83] have been measured for the allowed transitions ^2S–$^2P^o$ and ^2D–$^2P^o$, but not for the optically forbidden transition ^2S–^2D. The search for

numerical solutions with the observed agreement of the Boltzmann temperatures $kT_{6s5d}=kT_{6s6p}$ resulted in a lower limit for the threshold value $Q^o(^2S-^2D)=10^{-18}$ m^2 for the unknown collision cross section (at 140 ns, where $\bar{N}_e\simeq10^{20}$ m^{-3}). This cross-section value is reasonable, if compared with $Q^o(^2S-^2P^o)=5.7\times10^{-19}$ m^2 for the resonance transition, whose energy difference is four times as large.

The model calculations also showed that the lower bound $Q^o(^2S-^2D)=10^{-18}$ m^2 leads to a satisfactory agreement ($<15\%$) between electron and Boltzmann temperatures. Consequently, the observed rise of the Boltzmann temperatures from 0.29 to 0.44 eV between 140 and 400 ns (Fig. 6) can be regarded to reflect that of the electron temperature as well.

D. Excitation and ionization of strontium and calcium

Figure 7 shows that the populations of strontium are directly coupled to the electron density and temperature; the level $5p\,^3P_2^o$ ($E=1.85$ eV) reaches its maximum at about 370 ns, i.e., where kT_e and $\bar{N}_e$ are near their maximum values. We also note that the Boltzmann temperature as derived from the ratio $\bar{N}(5p\,^3P_2^o)/\bar{N}(5s^2\,^1S_0)$ is 0.42 ± 0.06 eV at 370 ns and agrees well with that measured from the Ba ions of 0.44 ± 0.03 eV (cf. Fig. 6).

The energy of the electron gas seems to be taken up by Sr as follows. During the first 400 ns the low-lying levels are excited and at the end of this phase they are in LTE with the ground state; the optically thick resonance line of Sr (the escape factor at our densities is of the order of 10^{-3}) contributes to the establishment of LTE. Efficient ionization occurs only for times greater than 400 ns.

In Sec. III A 1 we concluded that the maximum ionization of Sr reached $75\pm5\%$ at 1.8 μs, and that this ionization corresponded to an electron temperature of 0.40 ± 0.01 eV, in agreement with the value derived from Ba^+ at that time (cf. Fig. 6). The growth of the Sr ion density is also consistent with that observed for Ba^+: By adjusting the relative ion densities of Fig. 7 one obtains a growth rate for the Sr ions of about 9×10^{25} m^{-3}s^{-1} at 400 ns, i.e., about 28 times less than that for Ba^+ at 240 ns ($\simeq2.5\times10^{27}$ m^{-3}s^{-1}); this factor of ≈30 stems from the small population of the Sr resonance level which is about 60 times smaller ($\simeq3\times10^{17}$ m^{-3} at 400 ns assuming LTE) than in Ba ($\simeq1.8\times10^{19}$ m^{-3} at 240 ns), and from the electron density at 400 ns which is double that at 240 ns (cf. Fig. 6). As the term schemes of the two elements are very similar and the ionization energies out of the corresponding resonance levels differ by only 0.003 eV such a behavior could be expected. It should perhaps be mentioned here that the Sr line $4d\,^3D_3-5d'\,^3D_2^o$ ($\lambda=553.48$ nm) lies only 0.07 nm below the Ba resonance line, so that a further channel for efficient ionization is available in Sr as it was the case in Ba.

In calcium, no excitation could be detected. As reported in Sec. III A 1, the measuring errors connected with the small gound-state density ($\simeq1.2\times10^{18}$ m^{-3}) correspond to an excitation of less than 20% or an electron temperature $\lesssim0.36$ eV in LTE.

A LTE population of the low-lying Ca levels before onset of the efficient ionization—as it was observed in Sr around 400 ns—leads to 16.5% of excited Ca atoms at $kT_e=0.44$ eV. Such a change of the ground-state density is within the experimental errors, and could therefore not be established experimentally. Since the resonance line of calcium is not optically thick (escape factor ≈0.25), the population of the resonance level cannot reach its equilibrium value. This, together with the ionization energy being 0.42 eV larger than in Sr, may explain the absence of observable ionization in calcium.

Further ionization channels for Sr and Ca are charge-exchange collisions as, for instance, the following exothermic process starting from the strongly populated $5d\,^2D$ term in Ba^+:

$$Ba^+(5d\,^2D)+Sr(5s^2\,^1S_0)\rightarrow Ba(6s^2\,^1S_0)+Sr^+(5s\,^2S_{1/2})+0.18\text{ eV}.$$

As the cross section of this process has not been measured, we take the exothermic reaction $Na^+ + K \rightarrow Na + K^+ + 0.8$ eV for comparison; its rate coefficient at a thermal energy of 0.1 eV (1160 K) is about 7×10^{-15} m^{3}s^{-1}.[84]

The growth rate of the Sr ion density at 400 ns ($\simeq9\times10^{25}$ m^{-3}s^{-1}) could, in principle, be explained with charge-exchange collisions alone, if a rate coefficient of about 9×10^{-15} m^{3}s^{-1}, i.e., quite a realistic value, is assumed. In calcium, however, only the endothermic reaction

$$Ba^+(5d\,^2D)+Ca(4s^2\,^1S_0)\rightarrow Ba(6s^2\,^1S_0)+Ca^+(4s\,^2S_{1/2})-0.24\text{ eV}$$

is possible. A predominant ionization of the Sr and Ca impurities by charge-exchange collisions could therefore also be an explanation for the lack of ionization in calcium. Given the lack of measured cross sections for these charge-exchange processes, it is, however, not possible to establish the prevailing ionization mechanism.

V. CONCLUSION

With the present experiment we measured for the first time the temporal development of the population densities of all relevant levels in a laser-pumped Ba vapor with a time resolution of better than 5 ns. With our laser irradiance (7 GW m^{-2}) it was possible to excite the Ba vapor within 50 ns along the entire vapor column. This led to negligible density gradients along the optical axis.

With Ba vapor densities of $\approx6\times10^{20}$ m^{-3}, we found that 100 ns after the beginning of the resonant laser pulse, all levels lying below the resonance level were strongly populated and that the vapor was almost completely ionized after 400 ns. During the efficient ionization, between 200 and 400 ns, the high-lying levels exhibited a thermal population.

The strong density-dependence of the ionization efficiency suggests a collision-dominated ionization mechanism. Superelastic collisions of electrons with excited Ba atoms can provide the needed energy for excitation and ionization, if collisions with the laser-pumped *and* with the lower-lying metastable levels are taken into account.

The observed ionization rate could be explained by use of model calculations which considered electron-impact excitation of high-lying levels with subsequent electron-impact ionization as well as photoionization by the laser. In particular it turned out that the numerous, densely packed high-lying levels of Ba are important for the ionization speed; the excitation can rapidly "climb" up to the ionization limit in small steps.

In the course of this investigation, we noticed that the published oscillator strengths of transitions out of excited Ba levels had to be lowered by approximately a factor of 2.[35,36] The experimental method described, thus also provides a test for oscillator strengths. In summary, we present extensive observations and provide quantitative explanations of the process of resonant laser-excitation and -ionization in the case of barium.

ACKNOWLEDGMENTS

Professor R. J. Sandeman, who visited the Eidgenössische Technische Hochschule Zürich several times while this work was in progress, has made important contributions. We thank him for stimulating suggestions and hands-on guidance with some equipment, and Professor K. Dressler for his constant encouragement and support. The technical help of A. Wahl, F. Brunner, M. Ilg, C. Schönenberger, and P. Bocklet is gratefully acknowledged. We also acknowledge helpful discussions with Lady Anne P. Thorne and Dr. H.-A. Bachor, Dr. T. B. Lucatorto, Professor T. J. McIlrath, and Dr. J. E. G. Wheaton. This work was supported in part by the Schweizerischer Nationalfonds.

[1]T. B. Lucatorto and T. J. McIlrath, Phys. Rev. Lett. 37, 428 (1976).

[2]T. J. McIlrath and T. B. Lucatorto, Phys. Rev. Lett. 38, 1390 (1977).

[3]J. M. Salter, D. D. Burgess, and N. A. Ebrahim, J. Phys. B 12, L759 (1979).

[4]J. M. Salter, J. Phys. B 12, L763 (1979).

[5]F. Roussel, P. Breger, G. Spiess, C. Manus, and S. Geltman, J. Phys. B 13, L631 (1980).

[6]F. Roussel, B. Carré, P. Breger, and G. Spiess, J. Phys. B 14, L313 (1981).

[7]B. Carré, F. Roussel, P. Breger, and G. Spiess, J. Phys. B 14, 4271 (1981).

[8]B. Carré, F. Roussel, P. Breger, and G. Spiess, J. Phys. B 14, 4289 (1981).

[9]T. Stacewicz and J. Krasinski, Opt. Commun. 39, 35 (1981).

[10]C. H. Skinner, J. Phys. B 13, 55 (1980).

[11]C. Bréchignac and Ph. Cahuzac, Opt. Commun. 43, 270 (1982).

[12]C. Bréchignac and Ph. Cahuzac, in *Laser Spectroscopy VI, Proceedings of 6th International Conference, Interlaken, 1983,* Vol. 40 of *Springer Series in Optical Sciences,* edited by H. P. Weber and W. Lüthy (Springer, Berlin, 1983), p. 195.

[13]H.-A. Bachor and M. Kock, J. Phys. B 13, L369 (1980).

[14]H.-A. Bachor and M. Kock, J. Phys. B 14, 2793 (1981).

[15]H.-A. Bachor, PhD thesis, Universität Hannover, 1980 (unpublished).

[16]J. L. Bowen, PhD thesis, Imperial College, University of London, 1982 (unpublished).

[17]J. L. Bowen and A. P. Thorne (unpublished).

[18]T. B. Lucatorto and T. J. McIlrath, Appl. Opt. 19, 3984 (1980).

[19]R. M. Measures, J. Quant. Spectrosc. Radiat. Transfer 10, 107 (1970).

[20]R. M. Measures and P. G. Cardinal, Phys. Rev. A 23, 804 (1981).

[21]R. M. Measures, P. G. Cardinal, and G. W. Schinn, J. Appl. Phys. 52, 1269 (1981).

[22]C. H. Skinner, J. Phys. B 13, L637 (1980).

[23]T. J. McIlrath and T. B. Lucatorto, J. Phys. B 13, L641 (1980).

[24]J. L. Le Gouët, J. L. Picqué, F. Wuilleumier, J. M. Bizau, P. Dhez, P. Koch, and D. L. Ederer, Phys. Rev. Lett. 48, 600 (1982).

[25]J. M. Bizau, B. Carré, P. Dhez, D. L. Ederer, P. Gérard, J. C. Keller, P. Koch, J. C. Le Gouët, J. L. Picqué, F. Roussel, G. Spiess, and F. Wuilleumier, in *Laser Spectroscopy VI,* Ref. 12, p. 89.

[26]W. C. Marlow, Appl. Opt. 6, 1715 (1967).

[27]M. C. E. Huber, in *Modern Optical Methods in Gas Dynamic Research,* edited by D. S. Dosanjh (Plenum, New York, 1971), p. 85.

[28]M. Lambropoulos, Opt. Commun. 15, 35 (1975).

[29]K. L. Matheson and J. M. Thorne, Appl. Phys. Lett. 35, 314 (1979).

[30]W. Kinder, Optik (Stuttgart) 1, 413 (1946).

[31]R. J. Sandeman and N. A. Ebrahim, Appl. Opt. 16, 1376 (1977).

[32]W. R. S. Garton, J. P. Connerade, M. W. D. Mansfield, and J. E. G. Wheaton, Appl. Opt. 8, 919 (1969).

[33]Yu. G. Kozlov and G. A. Plekhotin, Opt. Spectrosc. 36, 600 (1974).

[34]R. J. Sandeman, Appl. Opt. 18, 3873 (1979).

[35]L. Jahreiss, PhD thesis, Eidgenössische Technische Hochschule Zürich, 1983 (unpublished).

[36]L. Jahreiss and M. C. E. Huber (unpublished).

[37]B. M. Miles and W. L. Wiese, At. Data 1, 1 (1969).

[38]W. H. Parkinson, E. M. Reeves, and F. S. Tomkins, J. Phys. B 9, 157 (1976).

[39]N. P. Penkin and L. N. Shabanova, Opt. Spectrosc. 12, 1 (1962).

[40]A. Gallagher, Phys. Rev. 157, 24 (1967).

[41]From the observed ratio of 3:1 (0.5 dex) between the populations of $6p\ ^1P_1^o$ and $6s^2\ ^1S_0$, i.e., the laser-excited level and the ground state (cf. Fig. 3), we concluded that the densities were high enough to equalize the populations among the three states of the $6p\ ^1P_1^o$ level. In the absence of collisions, the strong linear polarization of the pump laser would result in a predominant optical pumping of the state with $M_J=0$.

[42]Ba lasers operating on these two infrared lines are known (see Refs. 43–45).

[43]Ph. Cahuzac and X. Drago, Opt. Commun. 18, 600 (1976).

[44]B. G. Bricks, T. W. Karras, and R. S. Anderson, IEEE J. Quantum Electron. QE-13, 93D (1977).

[45]B. G. Bricks, T. W. Karras, and R. S. Anderson, J. Appl. Phys. 49, 38 (1978).

[46]The stray light of the pump laser prevented us from measuring

the expected blue emissions in the 3.4-m spectrograph.
[47]H. N. Russell and C. E. Moore, J. Res. Natl. Bur. Stand. (U. S.) 55, 299 (1955).
[48]Contributions of ionized strontium to the electron density (see below) are not included in the plotted $\bar{N}_e$.
[49]More detailed measurements are presented in Ref. 35.
[50]T. Holstein, Phys. Rev. 72, 1212 (1947).
[51]T. Holstein, Phys. Rev. 83, 1159 (1951).
[52]The populations shown in Fig. 12, that were derived from hook-interferometry-method data were adjusted, since the laser power used here was only 70% of the full laser power.
[53]Measurements of transitions from terms near the double of the excitation energy of the Ba resonance level did not reveal any enhanced fluorescence signals.
[54]Y. R. Shen, Prog. Quant. Electron. 4, 1 (1975).
[55]C. H. Skinner and P. D. Kleiber, Phys. Rev. A 21, 151 (1980).
[56]K. Shimoda, in *High Resolution Laser Spectroscopy,* Vol. 13 of *Topics in Applied Physics,* edited by K. Shimoda, (Springer, Berlin, 1976), p. 16.
[57]The irradiance of a rectangular pulse of 750-ns length is equal to the peak irradiance of our laser pulse (half-intensity width of 750 ns, cf. Fig 3), if both pulses have the same energy content.
[58]A. Yariv, *Introduction to Optical Electronics* (Holt, Rinehart and Winston, New York, 1971), p. 83.
[59]F. T. Arecchi and E. Courtens, Phys. Rev. A 2, 1730 (1970).
[60]R. Bonifacio, L. A. Lugiato, in *Dissipative Systems in Quantum Optics,* Vol. 27 of *Topics in Current Physics,* edited by R. Bonifacio (Springer, Berlin, 1982), p. 4.
[61]We estimate an f value of about 0.025 for this line from the value of 0.026 given by Miles and Wiese (Ref. 37) for the transition $5d\ ^3D_2$-$6p\ ^3P_1^o$ ($\lambda=2922.4$ nm) and based on the identical intensity value given by Russell and Moore (Ref. 47) for both lines.
[62]J. Huennekens and A. Gallagher, Phys. Rev. A 27, 771 (1983).
[63]V. M. Borodin and I. V. Komarov, Opt. Spectrosc. 36, 145 (1974).
[64]J. L. Carlsten and P. C. Dunn, Opt. Commun. 14, 8 (1975).
[65]M. Chéret, L. Barbier, W. Lindinger, and R. Deloche, J. Phys. B 15, 3463 (1982).
[66]M. Mitchner and C. H. Kruger, *Partially Ionized Gases* (Wiley, New York, 1973).
[67]F. Demmig, in *11th Shock Tube Symposium, Seattle, 1977,* edited by B. Ahlborn, A. Hertzberg, and D. Russell (University of Washington Press, Seattle, 1978), p. 119.
[68]S. T. Chen and A. Gallagher, Phys. Rev. A 14, 593 (1976).
[69]H. K. Holt and R. Krotkov, Phys. Rev. 144, 82 (1966).
[70]J. D. Jobe and R. M. St. John, Phys. Rev. 164, 117 (1967).
[71]H.-W. Drawin, Z. Phys. 164, 513 (1961).
[72]Y. Okuno, J. Phys. Soc. Jpn. 31, 1189 (1971).
[73]J.-M. Dettmann and F. Karstensen, J. Phys. B 15, 287 (1982).
[74]H.-W. Drawin and P. Felenbok, *Data for Plasmas in Local Thermodynamic Equilibrium* (Gauthier-Villars, Paris, 1965).
[75]I. S. Aleksakhin, S. B. Zagrebin, D. A. Ozolinsh, A. V. Samson, I. I. Shafranosh, and T. A. Shishova, Opt. Spectrosc. 53, 222 (1982).
[76]M. Aymar, R.-J. Champeau, C. Delsart, and J.-C. Keller, J. Phys. B 14, 4489 (1981).
[77]M. Aymar, P. Grafström, C. Levison, H. Lundberg, and S. Svanberg, J. Phys. B 15, 877 (1982).
[78]The f values calculated in this way for transitions with large energy gaps are much smaller than the measured ones (Ref. 37) (except for those involving the ground state). Oscillator strengths belonging to small energy differences (which have not been measured) may be too large, on the other hand. The derived cross sections are therefore not reliable, they may be too small or too large.
[79]J. L. Carlsten, T. J. McIlrath, and W. H. Parkinson, J. Phys. B 8, 38 (1975).
[80]J. F. Shaw, M. Mitchner, and C. H. Kruger, Phys. Fluids 13, 325 (1970).
[81]References 80 and 66 actually treat the opposite case, where the population temperatures are lower than the electron temperature. The adaption of the results to our case is straightforward however.
[82]E. B. Sonin, Zh. Eksp. Teor. Fiz. 54, 1554 (1968) [Sov. Phys.—JETP 27, 832 (1968)].
[83]D. H. Crandall, P. O. Taylor, and G. H. Dunn, Phys. Rev. A 10, 141 (1974).
[84]M. Riggin and M. Bloom, J. Chem. Phys. 63, 3046 (1975).